TEICHMÜLLER MAPPING (T-MAP) AND ITS APPLICATIONS TO LANDMARK MATCHING REGISTRATION

LOK MING LUI, KA CHUN LAM, SHING-TUNG YAU AND XIANFENG GU

Abstract. Registration, which aims to find an optimal 1-1 correspondence between shapes, is an important process in different research areas. Landmark-based surface registration have been widely studied to obtain a mapping between shapes that matches important features. Obtaining a unique and bijective surface registration that matches features consistently is generally challenging, especially when a large number of landmark constraints are enforced. This motivates us to search for a unique landmark-matching surface diffeomorphism, which minimizes the local geometric distortion. For this purpose, we propose to consider a special class of diffeomorphisms called the *Teichmüller mappings* (T-Maps). Under suitable condition on the landmark constraints, a unique T-Map between two surfaces can be obtained, which minimizes the maximal conformality distortion. The conformality distortion measures how far the mapping is deviated from a conformal mapping, and hence it measures the local geometric distortion. In this paper, we propose an efficient iterative algorithm, called the *Quasi-conformal (QC) iterations*, to compute the T-Map. The basic idea is to represent the set of diffeomorphisms using Beltrami coefficients (BCs), and look for an optimal BC associated to the desired T-Map. The associated diffeomorphism can be efficiently reconstructed from the optimal BC using the Linear Beltrami Solver(LBS). Using BCs to represent diffeomorphisms guarantees the diffeomorphic property of the registration, even with very large deformation. Using our proposed method, the T-Map can be accurately and efficiently computed. The obtained registration is guaranteed to be bijective. The proposed algorithm can also be extended to compute T-Map with soft landmark constraints. We applied the proposed algorithm to real applications, such as brain landmark matching registration, constrained texture mapping and human face registration. Experimental results shows that our method is both effective and efficient in computing a non-overlap landmark matching registration with least amount of conformality distortion.

Key words. Teichmüller mapping, Beltrami coefficient, conformality distortion, Linear Beltrami Solver, Landmark matching registration

1. Introduction.

Registration refers to the process of finding an optimal one-to-one correspondence between images or surfaces. It has been extensively applied to different areas such as medical imaging, computer graphics and computer visions. For example, in medical imaging, registration is always needed for statistical shape analysis, morphometry and processing of signals on brain surfaces (e.g., denoising or filtering). While in computer graphics, surface registration is needed for texture mapping, which aligns each vertex to a position of the texture image, to improve the visualization of the surface mesh. Developing an effective algorithm for registration is therefore very important.

Landmark-based registration have been widely studied to obtain a smooth 1-1 correspondence between different domains that matches important features. This kind of registration, with good feature alignment, is particularly crucial in medical imaging, computer visions and computer graphics. For example, in medical imaging, anatomical features in brain cortical surfaces can be systematically delineated, such as sulci (the fissures in the brain surface). Landmark matching brain registration is often required to obtain a meaningful 1-1 correspondence between brain surfaces, so that further analysis can be carried out (e.g. building surface average of many subjects). However, obtaining a unique and bijective registration that matches features consistently is generally challenging, especially when a large number of landmark constraints are enforced. Motivated by this, we are interested in searching for a *unique* and *bijective landmark-matching* diffeomorphism, associated with a given landmark constraints, which minimizes the local geometric distortion.

In this paper, we propose to consider a special class of diffeomorphisms called

the *Teichmüller mappings* (T-Map), which have uniform conformality distortion over the whole domain (See Figure 3.3). Under suitable conditions on the landmark constraints, there exists a unique T-Map between two surfaces, which minimizes the maximal conformality distortion. The conformality distortion measures how far the mapping is deviated from a conformal mapping, and hence it measures the local geometric distortion. To compute this T-Map, we propose in this paper an efficient and effective iterative algorithm, which is called the *Quasi-conformal (QC) iterations*. The basic idea is to represent the set of diffeomorphisms using Beltrami coefficients (BCs), and look for an optimal BC associated to the desired T-Map. The associated T-Map can then be efficiently computed from the optimal BC using the Linear Beltrami Solver(LBS).

Using the T-Map for landmark matching registration is advantegous for the following reasons:

1. **Optimized conformality distortion:** Given a set of landmark constraints, our algorithm is able to determine an optimal 1-1 correspondence between shapes automatically, which minimizes the conformality distortion. In the case of open surfaces with boundaries, the proposed algorithm can also automatically determine the optimal boundary correspondence that minimizes the maximal conformality distortion. Hence, Dirichlet boundary condition is not required (which is usually needed for other algorithms such as harmonic registration).

2. **Bijectivity:** Another major advantage of using T-Maps for landmark matching registrations is that the bijectity (1-1, onto) of the registrations can be guaranteed. Obtaining a bijective landmark matching registration is generally difficult, especially when a large number of landmark constraints are enforced. Using our proposed method, a bijective T-Map can be computed, even with large deformation or large number of landmarks (See Figure 6.6).

3. **Uniqueness:** Besides, the mapping is uniquely determined. In other words, every prescribed landmark constraints is associated with a unique T-Map.

4. **Extension to soft landmark constraints:** The proposed algorithm can also be extended to compute T-Maps with soft landmark constraints. It becomes necessary when landmark features cannot be accurately located, and hence it is better to compute registration with landmarks approximately (but not exactly) matched (See Figure 6.7).

5. **Independence of mesh structure:** The proposed QC iterations rely on the Linear Beltrami Solver. The Linear Beltrami Solver computes the associated piecewise linear map between meshes with a given beltrami coefficient defined on each face. The solver is independent of the mesh structure. Hence, our algorithm can compute a bijective landmark matching registration between meshes even with irregular mesh structure (See Figure 5.4).

6. **Fast computation:** The QC iterations involve solving a sparse symmetric positive definite linear system in each iterations. The linear system can be solved quickly, and the iterations converge quickly. Using our proposed method, the T-Map can be efficiently computed, even with dense meshes.

To test the effectiveness of our method, we applied the proposed algorithm to real applications, such as brain registration, constrained texture mapping and human face registration. Experimental results shows that our method is both effective and efficient in computing a non-overlap landmark matching registration with least amount of conformality distortion.

In short, the contributions of this paper are three-folded. Firstly, we propose an efficient algorithm for obtaining the unique *Teichmüller mapping* (T-Map) between shapes with landmark constraints enforced. The mapping is guaranteed to be bijective and minimizes the maximal conformality distortion. Secondly, we propose an algorithm to compute the T-Map with soft landmark constraints. Landmarks are not exactly matched, but less conformality distortion will be introduced. Thirdly, we apply the proposed algorithms to real applications, namely, constrained texture mapping, medical image registration and human face registration.

2. Previous work. Surface registration has been extensive studied and various algorithms have been proposed by different research groups. In this section, we will extract some previous works most closely related to our paper.

- **Landmark-free surface registration:** Landmark-free registration has been proposed to obtain 1-1 correspondences between shapes without feature landmarks. Different algorithms have been proposed to obtain registrations based on the shape information (such as curvatures) defined on the surfaces. Lyttelton et al. [4] computed surface parameterizations with surface curvature matching. Fischl et al. [6] proposed an algorithm for brain registration that better align cortical folding patterns, by minimizing the mean squared difference between the convexity of the surface and the average convexity across a set of subjects. Lord et al. [16] proposed to match surfaces by minimizing the deviation of the registration from isometry. Yeo et al. [18] proposed the spherical demons method, which adopted the diffeomorphic demons algorithm [17], to drive surfaces into correspondence based on the mean curvature and average convexity.

  Conformal surface registration, which minimizes angular distortions, has also been widely used to obtain a smooth 1-1 correspondence between surfaces [3, 7, 9, 8, 15, 41, 42, 43]. An advantage of conformal registrations is that they preserve local geometry well. However, it cannot map landmark features, such as sulcal landmarks on brain surfaces, consistently.

  Sometimes, deformations between objects might not be conformal. Instead, certain amount of angular distortion could be introduced. To tackle with this situation, quasi-conformal mappings have been applied to obtain smooth 1-1 correspondences with bounded conformality distortion [26, 27, 28, 29, 45]. The obtained registration can match the geometric quantities (such as curvature), while minimizing the maximal dilation of the mapping.

- **Landmark-based surface registration:** Most of the above registration algorithms cannot match feature landmarks, such as sulcal landmarks on the human brains, consistently. To alleviate this issue, landmark-matching registration algorithms are proposed by various research groups. Bookstein et al. [19] proposed to obtain a registration that matches landmarks as much as possible using a thin-plate spline regularization (or biharmonic regularization). Wang et al. [20, 21, 22, 23] proposed to compute the optimized conformal parameterizations of brain surfaces by minimizing a compounded energy [20, 23]. The obtained registration can obtain an optimized harmonic map that better aligns the features, however, landmarks cannot be exactly matched. Besides, bijectivity cannot be ensured when large number of landmark constraints are enforced. Tosun et al. [39] proposed to combine iterative closest point

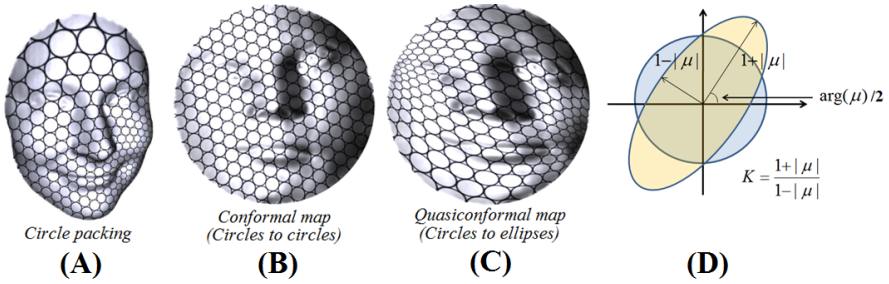

FIG. 2.1. *(A) shows a human face with circle packing texture. Under the conformal parameterization, infinitesimal circles are mapped to circles as shown in (B). Under quasi-conformal parameterization, infinitesimal circles are mapped to ellipse as shown in (C). (D) illustrates how the Beltrami coefficient measure the conformality distortion of a quasi-conformal map.*

registration, parametric relaxation and inverse stereographic projection to align cortical sulci across brain surfaces. These diffeomorphisms obtained can better match landmark features, although not perfectly. Later, Lin et al. [44] propose a unified variational approach for registration of gene expression data to neuroanatomical mouse atlas in two dimensions that matches feature landmarks. Again, landmarks cannot be exactly matched. Note that inexact landmark-matching registrations are sometimes beneficial. In the case when landmark points/curves are not entirely accurate, this method is more tolerant of errors in labeling landmarks and gives better parameterization.

In the situation when exact landmark matching is required, smooth vector field has been applied to obtain surface registration. Lui et al. [21, 22] proposed the use of vector fields to represent surface maps and reconstruct them through integral flow equations. They obtained shape-based landmark matching harmonic maps by looking for the best vector fields minimizing a shape energy. The use of vector fields to compute the registration makes the optimization easier, although it cannot describe all surface maps. An advantage of this method is that exact landmark matching can be guaranteed. Time dependent vector fields can also be used [10, 11, 12, 13, 14]. For example, Glaunés et al. [11] proposed to generate large deformation diffeomorphisms of a sphere, with given displacements of a finite set of template landmarks. The time dependent vector fields facilitate the optimization procedure, although it may not be a good representation of surface maps since it requires more memory. The computational cost of the algorithm is also expensive.

Quasi-conformal mapping that matches landmarks consistently has also been proposed[26, 40]. In [26], the authors proposed to compute the brain landmark-matching registration, which minimizes L^2 norm of the Beltrami coefficients. Wei et al. [40] also proposed to compute quasi-conformal mappings for feature matching face registration. The Beltrami coefficient associated to a landmark points matching parameterization is approximated. However, either exact landmark matching or the bijectivity of the mapping cannot be guaranteed, especially when very large deformations occur.

3. Mathematical Background. In this section, we describe some basic mathematical concepts related to our algorithms. For details, we refer the readers to [5, 30, 31].

A surface S with a conformal structure is called a *Riemann surface*. Given two Riemann surfaces M and N, a map $f : M \to N$ is *conformal* if it preserves the surface metric up to a multiplicative factor called the *conformal factor*. An immediate consequence is that every conformal map preserves angles. With the angle-preserving property, a conformal map effectively preserves the local geometry of the surface structure.

A generalization of conformal maps is the *quasi-conformal* maps, which are orientation preserving homeomorphisms between Riemann surfaces with bounded conformality distortion, in the sense that their first order approximations takes small circles to small ellipses of bounded eccentricity [5]. Mathematically, $f\colon \mathbb{C} \to \mathbb{C}$ is quasi-conformal provided that it satisfies the Beltrami equation:

$$\frac{\partial f}{\partial \overline{z}} = \mu(z)\frac{\partial f}{\partial z}. \tag{3.1}$$

for some complex-valued function μ satisfying $||\mu||_\infty < 1$. μ is called the *Beltrami coefficient*, which is a measure of non-conformality. It measures how far the map at each point is deviated from a conformal map. In particular, the map f is conformal around a small neighborhood of p when $\mu(p) = 0$. Infinitesimally, around a point p, f may be expressed with respect to its local parameter as follows:

$$\begin{aligned} f(z) &= f(p) + f_z(p)z + f_{\overline{z}}(p)\overline{z} \\ &= f(p) + f_z(p)(z + \mu(p)\overline{z}). \end{aligned} \tag{3.2}$$

Obviously, f is not conformal if and only if $\mu(p) \neq 0$. Inside the local parameter domain, f may be considered as a map composed of a translation to $f(p)$ together with a stretch map $S(z) = z + \mu(p)\overline{z}$, which is postcomposed by a multiplication of $f_z(p)$, which is conformal. All the conformal distortion of $S(z)$ is caused by $\mu(p)$. $S(z)$ is the map that causes f to map a small circle to a small ellipse. From $\mu(p)$, we can determine the angles of the directions of maximal magnification and shrinking and the amount of them as well. Specifically, the angle of maximal magnification is $\arg(\mu(p))/2$ with magnifying factor $1 + |\mu(p)|$; The angle of maximal shrinking is the orthogonal angle $(\arg(\mu(p)) - \pi)/2$ with shrinking factor $1 - |\mu(p)|$. Thus, the Beltrami coefficient μ gives us all the information about the properties of the map (See Figure 2.1(D)).

The maximal dilation of f is given by:

$$K(f) = \frac{1 + ||\mu||_\infty}{1 - ||\mu||_\infty}. \tag{3.3}$$

Let $f = u + \sqrt{-1}v$. From the Beltrami equation (3.1),

$$\mu(f) = \frac{(u_x - v_y) + \sqrt{-1}\ (v_x + u_y)}{(u_x + v_y) + \sqrt{-1}(v_x - u_y)} \tag{3.4}$$

Let $\mu(f) = \rho + \sqrt{-1}\ \tau$. We can write v_x and v_y as linear combinations of u_x and u_y,

$$\begin{aligned} -v_y &= \alpha_1 u_x + \alpha_2 u_y; \\ v_x &= \alpha_2 u_x + \alpha_3 u_y. \end{aligned} \tag{3.5}$$

where $\alpha_1 = \frac{(\rho-1)^2+\tau^2}{1-\rho^2-\tau^2}$; $\alpha_2 = -\frac{2\tau}{1-\rho^2-\tau^2}$; $\alpha_3 = \frac{1+2\rho+\rho^2+\tau^2}{1-\rho^2-\tau^2}$.

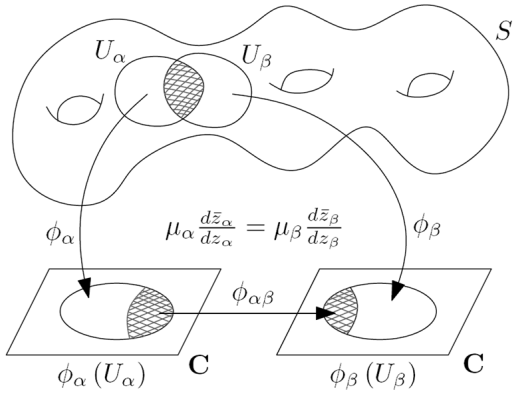

FIG. 3.1. *Illustration of how Beltrami differential is defined on general Riemann surfaces.*

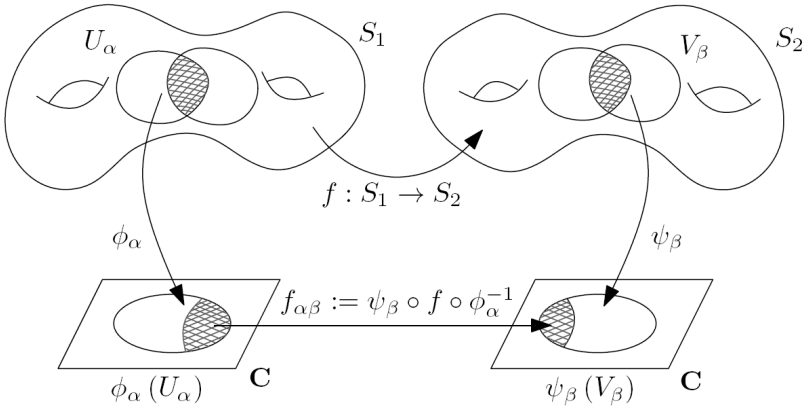

FIG. 3.2. *Illustration of quasi-conformal mapping between Riemann surfaces.*

Similarly,

$$\begin{aligned} -u_y &= \alpha_1 v_x + \alpha_2 v_y; \\ u_x &= \alpha_2 v_x + \alpha_3 v_y. \end{aligned} \tag{3.6}$$

Since $\nabla \cdot \begin{pmatrix} -v_y \\ v_x \end{pmatrix} = 0$, we obtain

$$\nabla \cdot \left(A \begin{pmatrix} u_x \\ u_y \end{pmatrix} \right) = 0 \quad \text{and} \quad \nabla \cdot \left(A \begin{pmatrix} v_x \\ v_y \end{pmatrix} \right) = 0 \tag{3.7}$$

where $A = \begin{pmatrix} \alpha_1 & \alpha_2 \\ \alpha_2 & \alpha_3 \end{pmatrix}$.

In this paper, a discrete version of equation (3.7) for a piecewise linear mapping between meshes will be developed to compute the quasiconformal mapping (See Section 5.1).

Quasiconformal mapping between two Riemann surfaces S_1 and S_2 can also be defined. Instead of the Beltrami coefficient, the *Beltrami differential* is used. A

Beltrami differential $\mu(z)\frac{\overline{dz}}{dz}$ on a Riemann surface S is an assignment to each chart (U_α, ϕ_α) of an L_∞ complex-valued function μ_α, defined on local parameter z_α such that

$$\mu_\alpha(z_\alpha)\frac{d\overline{z_\alpha}}{dz_\alpha} = \mu_\beta(z_\beta)\frac{d\overline{z_\beta}}{dz_\beta}, \tag{3.8}$$

on the domain which is also covered by another chart (U_β, ϕ_β). Here, $\frac{dz_\beta}{dz_\alpha} = \frac{d}{dz_\alpha}\phi_{\alpha\beta}$ and $\phi_{\alpha\beta} = \phi_\beta \circ \phi_\alpha^{-1}$ (See Figure 3.1).

An orientation preserving diffeomorphism $f : S_1 \to S_2$ is called quasi-conformal associated with $\mu(z)\frac{\overline{dz}}{dz}$ if for any chart (U_α, ϕ_α) on S_1 and any chart (V_β, ψ_β) on S_2, the mapping $f_{\alpha\beta} := \psi_\beta \circ f \circ f_\alpha^{-1}$ is quasi-conformal associated with $\mu_\alpha(z_\alpha)\frac{d\overline{z_\alpha}}{dz_\alpha}$ (See Figure 3.2).

In case S_1 and S_2 are simply-connected, conformal mapping between S_1 and S_2 always exists. However, conformal mapping may not exist between surfaces with complicated topology. For example, there is generally no conformal mapping between multiply-connected open surfaces (e.g. two annuli with different radii of inner circles). One would therefore be interested in finding an optimal quasi-conformal mapping that minimizes the confomrality distortion. More specifically, it is desirable to obtain an extremal quasiconformal mapping, which is extremal in the sense of minimizing the $||\cdot||_\infty$ over all Beltrami differentials corresponding to quasi-conformal mappings between S_1 and S_2. Extremal mapping always exists but need not to be unique. Mathematically, an extremal quasi-conformal mapping can be defined as follows:

Definition 3.1. *Let $f : S_1 \to S_2$ be a quasi-conformal mapping between S_1 and S_2. f is said to be an extremal mapping if for any quasi-conformal mapping $h : S_1 \to S_2$ isotopic to ϕ relative to the boundary,*

$$K(\phi) \leq K(\psi) \tag{3.9}$$

It is uniquely extremal if the inequality (3.9) is strict.

Another kind of mapping, called the *Teichmüller mapping*, is closely related to the extremal mapping. Teichmüller mapping is defined as follows:

Definition 3.2. *Let $f : S_1 \to S_2$ be a quasi-conformal mapping. f is said to be a Teichmüller mapping associated to the integrable holomorphic function $\varphi : S_1 \to \mathbb{C}$ if its associated Beltrami differential is of the form:*

$$\mu(f) = k\frac{\overline{\varphi}}{|\varphi|} \tag{3.10}$$

for some constant $k < 1$ and holomorphic function $\varphi \neq 0$ with $||\varphi||_1 = \int_{S_1} |\varphi| < \infty$.

It means a Teichmüller mapping is a quasiconformal mapping whose BC has a constant norm. Thus it has a uniform conformality distortion over the whole domain (See Figure 3.3).

Extremal mapping might not be unique. However, a Teichmüller mapping associated with a holomorphic function is the unique extremal mapping in its homotopic

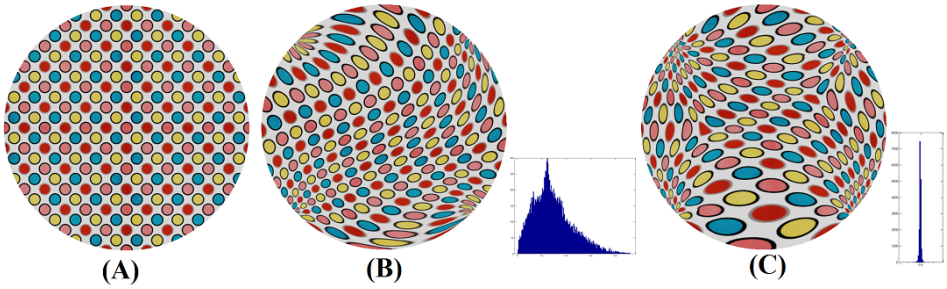

FIG. 3.3. *Difference between a general QC map and a Teichmüller map. (A) shows the original textured mesh. It is mapped to another disk by a general QC map. Note that the distribution of the norm of BC are spread out. (C) shows the Teichmüller map, whose BC norm is concentrated near 0.4.*

class. The Strebel's theorem explains the relationship bewtween the Teichmüller mapping and extremal mapping.

Definition 3.3 (Boundary dilation). *Suppose S_1 and S_2 are open Riemann surfaces with the same topology. The boundary dilation $K_1[f]$ of f is defined as:*

$$K_1[f] = \inf_C \{K(h|_{S_1 \setminus C}) : h \in \mathfrak{F}, C \subseteq S_1, C \text{ is compact.}\} \tag{3.11}$$

where $\mathfrak{F}$ is the family of quasi-conformal homeomorphisms of S_1 onto S_2 which are homotopic to f modulo the boundary.

Theorem 3.4 (Strebel's theorem, See [46], page 319). *Let f be an extremal quasi-conformal mapping with $K(f) > 1$. If $K_1[f] < K(f)$, then f is a Teichmüller map associated with an integrable holomorphic function on S_1. Hence, f is also an unique extremal mapping.*

In other words, an extremal mapping between S_1 and S_2 with suitable boundary condition is a Teichmüller mapping. In particular, the Teichmüller mapping and extremal mapping of the unit disk are closely related.

Theorem 3.5 (See [47], page 110). *Let $g : \partial\mathbb{D} \to \partial\mathbb{D}$ be an orientation-preserving homeomorphism of $\partial\mathbb{D}$. Suppose further that $h'(e^{i\theta}) \neq 0$ and $h''(e^{i\theta})$ is bounded. Then there is a Teichmüller mapping f that is the unique extremal extension of g to $\mathbb{D}$. That is, $f : \mathbb{D} \to \mathbb{D}$ is an extremal mapping with $f|_{\partial\mathbb{D}} = g$.*

Thus, if the boundary correspondence satisfies certain conditions on its derivatives, the extremal map of the unit disk must be a Teichmüller mapping.

Now, in the case when interior landmark constraints are further enforced, the existence of unique Teichmüller mapping can be guaranteed if the boundary and landmark correspondence satisfy suitable conditions. The unique Teichmüller mapping is extremal, which minimizes the maximal conformality distortion. The following theorem can be derived immediately from the Strebel's Theorem (Theorem 3.4):

Theorem 3.6 (Landmark-matching Teichmüller mapping). *Let S_1 and S_2 be open Riemann surfaces with the same topology. Let $\{p_i\}_{i=1}^n \in S_1$ and $\{q_i\}_{i=1}^n \in S_2$ be*

the corresponding interior landmark constraints. Let $f : S_1 \setminus \{p_i\}_{i=1}^n \to S_2 \setminus \{q_i\}_{i=1}^n$ *be the extremal quasi-conformal mapping, such that* p_i *corresponds to* q_i *for all* $1 \leq i \leq n$. *If* $K_1[f] < K(f)$, *then* f *is a Teichmüller map associated with an integrable holomorphic function on* $S_1 \setminus \{p_i\}_{i=1}^n$. *Hence,* f *is an unique extremal mapping.*

In particular, a unique Teichmüller mapping $f : \mathbb{D} \to \mathbb{D}$ between unit disks with interior landmark constraints enforced exists, if the boundary map $f|_{\partial\mathbb{D}}$ satisfies suitable conditions. The following theorem can be obtained directly from Theorem 3.5:

Theorem 3.7 (Landmark-matching Teichmüller mapping of $\mathbb{D}$). *Let* $g : \partial\mathbb{D} \to \partial\mathbb{D}$ *be an orientation-preserving homeomorphism of* $\partial\mathbb{D}$. *Suppose further that* $h'(e^{i\theta}) \neq 0$ *and* $h''(e^{i\theta})$ *is bounded. Let* $\{p_i\}_{i=1}^n \in \mathbb{D}$ *and* $\{q_i\}_{i=1}^n \in \mathbb{D}$ *be the corresponding interior landmark constraints. Then there is a Teichmüller mapping* $f : \mathbb{D} \setminus \{p_i\}_{i=1}^n \to \mathbb{D} \setminus \{q_i\}_{i=1}^n$ *matching the interior landmarks, which is the unique extremal extension of* g *to* $\mathbb{D}$. *That is,* $f : \mathbb{D} \setminus \{p_i\}_{i=1}^n \to \mathbb{D} \setminus \{q_i\}_{i=1}^n$ *is an extremal Teichmüller mapping with* $f|_{\partial\mathbb{D}} = g$ *matching the interior landmarks.*

Theorem 3.6 and 3.7 play the fundamental role for us to obtain a unique Teichmüller mapping between surfaces that matches feature landmarks consistently. We can therefore obtain a unique landmark matching registration by searching for an optimal Beltrami coefficient whose maximal dilatation is the minimum, while its norm is constant everywhere. In this paper, we abbreviate the Teichmüller mapping by T-Map.

It turns out that in most situations, an extremal quasi-conformal mapping is a T-Map (even for domains with non-trivial topologies). In some rare situations when an extremal mapping is not exactly a T-Map, one can still get a T-Map whose dilation is arbitrarily close to the extremal dilation.

Theorem 3.8. *(See [46], page 320) Let* $\mathfrak{F}$ *be a class of quasi-conformal mappings between the open Riemann surfaces* S_1 *and* S_2, *which are homotopic modulo the boundary. Let* K_0 *be the smallest maximal dilation of the mappings in* $\mathfrak{F}$. *Then there are T-Maps in* $\mathfrak{F}$, *associated with a meromorphic function with at most one simple pole, whose dilation is arbitrarily close to* K_0.

4. Variational Formulation. In this section, we give a variational formulation for obtaining the T-Map with least amount of conformality distortion. We propose to use the Beltrami coefficient(BC) to represent the mapping, instead of the commonly used representations by deformation fields or coordinate functions. The diffeomorphic property of the mapping can then be effectively controlled. Our goal is to formulate the problem into a variational framework to obtain an optimal BC, $\mu(f)$, associated to the desired T-Map f.

Suppose D_1 and D_2 are two domains in the complex plane with the same topology. D_1 and D_2 can either be simply-connected or multiply-connected. Suppose the boundary condition of the desired T-Map $f : D_1 \to D_2$ is known. Denote it by $f|_{\partial D_1} : \partial D_1 \to \partial D_2 = g$. Mathematically, the T-Map can be described as follows:

$$\frac{\partial f}{\partial \overline{z}} = k \frac{\overline{\varphi}}{|\varphi|} \frac{\partial f}{\partial z} \quad \text{and} \quad f|_{\partial D_1} = g \quad \text{on } \partial D_1 \tag{4.1}$$

for some constant k and integrable holomorphic function $\varphi : D_1 \to \mathbb{C}$ ($\varphi \neq 0$).

Recall that a T-Map is extremal in the sense that it minimizes the $||\cdot||_\infty$ over all Beltrami differentials corresponding to quasi-conformal mappings in the Teichmüller equaivalence class. In other words, for any $h : D_1 \to D_2$ satisfying $h|_{\partial D_1} = g$, we have

$$||\mu(f)||_\infty \leq ||\mu(h)||_\infty \tag{4.2}$$

where $\mu(f)$ and $\mu(h)$ are the Beltrami coefficient of f and h respectively. Hence, our original problem (4.1) can be formulated into a variational problem as follows:

$$\begin{aligned} f &= \mathbf{argmin}_{f:D_1\to D_2} E_1(f) \\ &:= \mathbf{argmin}_{f:D_1\to D_2}\{||\mu(f)||_\infty\} \end{aligned} \tag{4.3}$$

subject to:

- $f|_{\partial D_1} = g$ (boundary condition);
- $\mu(f) = k\frac{\overline{\varphi}}{\varphi}$ for some constant $0 \geq k < 1$ and holomorphic function $\varphi : D_1 \to \mathbb{C}$.

Theoretically, a diffeomorphism f is associated to a unique BC $\mu(f)$ with $||\mu(f)||_\infty < 1$. The Beltrami coefficient $\mu(f)$ measures the conformality distortion of the map f. It can be considered as a unique representation of f. The energy functional E_1 aims to minimize the maximal conformality distortion of the mapping.

However, minimizing $E_1(f)$ with respect to the space of all diffeomorphisms between D_1 and D_2 is difficult. More specifically, the variational problem (4.3) can be expressed as the following complicated form:

$$\begin{aligned} f &= \mathbf{argmin}_f\{||\mu(f)||_\infty\} \\ &= \mathbf{argmin}_f||\frac{\partial f/\partial\overline{z}}{\partial f/\partial z}||_\infty \end{aligned} \tag{4.4}$$

subject to $f|_{\partial D_1} = g$ and $\mu(f) = k\frac{\overline{\varphi}}{\varphi}$ for some constant $0 \geq k < 1$ and holomorphic function $\varphi : D_1 \to \mathbb{C}$.

In order to minimize the above constrained minimization problem effectively, we propose to reformulate the energy functional with respect to space of all Beltrami coefficients:

$$\begin{aligned} (\nu, f) &= \mathbf{argmin}_{\nu:D_1\to\mathbb{C}} E_2(\nu) \\ &:= \mathbf{argmin}_{\nu:D_1\to\mathbb{C}}\{||\nu||_\infty\} \end{aligned} \tag{4.5}$$

subject to:

- $\nu = \mu(f)$ and $||\nu||_\infty < 1$;
- $\nu = k\frac{\overline{\varphi}}{\varphi}$ for some constant $0 \geq k < 1$ and holomorphic function $\varphi : D_1 \to \mathbb{C}$;
- $f|_{\partial D_1} = g$ (boundary condition).

In other words, the minimization problem (4.3) is reformulated into an optimization problem over the space of all BCs, which are complex-valued functions defined

on D_1. Minimizing the energy functional with respect to BCs is advantageous since the diffeomorphic property of the mapping can be easily controlled [26]. Every diffeomorphism is associated to a smooth Beltrami coefficient $\mu(f)$. $\mu(f)$ measures the bijectivity (1-1 and onto) of f. In fact, $\mu(f)$ is related to the Jacobian $J(f)$ of f by the following formula:

$$|J(f)|^2 = |\frac{\partial f}{\partial z}|^2(1 - |\mu(f)|^2) \tag{4.6}$$

Therefore, the map f is bijective if $|\mu(f)|$ is everywhere less than 1. When solving the minimization problem (4.5), the bijectivity of the mapping in each iterations can be ensured by enforcing $||\nu||_\infty < 1$. Our goal is to look for an optimal BC, ν, such that its associated quasi-conformal map is our desired T-Map.

The boundary condition in the variational problem (4.5) can be relaxed. The Dirichlet condition defined on the whole boundary is not required. Also, interior landmark constraints can be enforced. Our goal is to solve the variational problem with these landmark constraints, which determines the optimal 1-1 correspondence (including the boundary correspondence) automatically. In other words, the boundary condition in the problem (4.5) can be reformulated as:

$$f(a_i) = b_i;\ f(p_j) = q_j;\ \text{for } i = 1, ..., n;\ j = 1, ..., m \tag{4.7}$$

where a_i and b_i are corresponding landmark points or curves defined on ∂D_1 and ∂D_2 respectively; and p_j and q_j are corresponding interior landmark points or curves in D_1 and D_2 respectively. By optimizing the energy functional (4.5), the landmark matching T-Map can be obtained, which matches landmark features consistently while minimizing the maximal conformality distortion.

Note also that the above formulation is designed for obtaining the T-Map of 2D connected domains. However, it can easily be extended to simply-connected or multiply-connected open surfaces. Let S_1 and S_2 be two connected open surfaces with the same topology. We can conformally parameterize S_1 and S_2 by $\phi_1 : S_1 \to D_1 \subset \mathbb{C}$ and $\phi_2 : S_2 \to D_2 \subset \mathbb{C}$ respectively. Then the T-Map $f : S_1 \to S_2$ between S_1 and S_2 induces the T-Map $\tilde{f} := \phi_2 \circ f \circ \phi_1^{-1} : D_1 \to D_2$. All the above formulation applies to $\tilde{f}$. In other words, the computation of the T-Map between connected surfaces embedded in $\mathbb{R}^3$ can be reduced to the computation of the T-Map between the conformal domains in $\mathbb{C}$.

In the subsequent section, we propose an algorithm, called the *quasi-conformal (QC) iteration* to solve the above minimization problems (4.5).

5. Main Algorithm. In this section, we describe an iterative scheme, called the *quasi-conformal (QC) iteration*, for solving the variational problem (4.5). The QC iteration is based on the Linear Beltrami Solver(LBS). The LBS will firstly be explained in detail. QC iteration will then be described.

Practically speaking, 2D domains or surfaces in $\mathbb{R}^3$ are usually represented discretely by triangular meshes. Suppose K_1 and K_2 are two surface meshes with the same topology representing S_1 and S_2. We define the set of vertices on K_1 and K_2 by $V^1 = \{v_i^1\}_{i=1}^n$ and $V^2 = \{v_i^2\}_{i=1}^n$ respectively. Similarly, we define the set of triangular faces on K_1 and K_2 by $F^1 = \{T_j^1\}_{j=1}^m$ and $F^2 = \{T_j^2\}_{j=1}^m$. Our goal is to look for a piecewise linear homeomorphism between K_1 and K_2 that approximates the T-Map between S_1 and S_2.

5.1. Linear Beltrami Solver. Our goal is to look for an optimal Beltrami coefficient(BC) associated to the desired T-Map. Every quasi-conformal mapping is associated to a unique BC. Given a BC, it is important to have an algorithm to reconstruct the associated quasi-conformal homeomorphism.

Suppose $f : K_1 \to K_2$ is an orientation preserving piecewise linear homeomorphism between K_1 and K_2. We can assume K_1 and K_2 are both embedded in $\mathbb{R}^2$. In case K_1 and K_2 are surface meshes in $\mathbb{R}^3$, we first parameterize them conformally by $\phi_1 : K_1 \to D_1 \subseteq \mathbb{R}^2$ and $\phi_2 : K_2 \to D_2 \subseteq \mathbb{R}^2$. The composition of f with the conformal parameterizations, $\tilde{f} := \phi_2 \circ f \circ \phi_1^{-1}$, is then an orientation preserving piecewise linear homeomorphism between D_1 and D_2 embedded in $\mathbb{R}^2$. In this paper, we assume the topology of the surface mesh is either a connected open surface or a genus-0 closed surface. In other words, the conformal domain D_i $(i = 1, 2)$ can either be a 2D rectangle, unit disk, punctual disk or unit sphere.

To compute the quasi-conformal mapping, the key idea is to discretize Equation 3.7 with two linear systems.

Given a map $f = (u + \sqrt{-1}v) : K_1 \to K_2$, we can easily compute its associated Beltrami coefficient μ_f, which is a complex-valued function defined on each triangular faces of K_1. To compute μ_f, we simply need to approximate the partial derivatives at every face T. We denote them by $D_x f(T) = D_x u + \sqrt{-1}D_x v$ and $D_y f(T) = D_y u + \sqrt{-1}D_y v$ respectively. Note that f is piecewise linear. The restriction of f on each triangular face T can be written as:

$$f|_T(x, y) = \begin{pmatrix} a_T x + b_T y + r_T \\ c_T x + d_T y + s_T \end{pmatrix} \tag{5.1}$$

Hence, $D_x u(T) = a_T$, $D_y u(T) = b_T$, $D_x v(T) = c_T$ and $D_y v(T) = d_T$. Now, the gradient $\nabla_T f := (D_x f(T), D_y f(T))^t$ on each face T can be computed by solving the linear system:

$$\begin{pmatrix} \vec{v}_1 - \vec{v}_0 \\ \vec{v}_2 - \vec{v}_0 \end{pmatrix} \nabla_T \tilde{f}_i = \begin{pmatrix} \frac{\tilde{f}_i(\vec{v}_1) - \tilde{f}_i(\vec{v}_0)}{|\vec{v}_1 - \vec{v}_0|} \\ \frac{\tilde{f}_i(\vec{v}_2) - \tilde{f}_i(\vec{v}_0)}{|\vec{v}_2 - \vec{v}_0|} \end{pmatrix}, \tag{5.2}$$

where $[\vec{v_0}, \vec{v_1}]$ and $[\vec{v_0}, \vec{v_2}]$ are two edges on T. By solving equation 5.2, a_T, b_T, c_T and d_T can be obtained. The Beltrami coefficient $\mu_f(T)$ of the triangular face T can then be computed from the Beltrami equation 3.1 by:

$$\mu_f(T) = \frac{(a_T - d_T) + \sqrt{-1}(c_T + b_T)}{(a_T + d_T) + \sqrt{-1}(c_T - b_T)}, \tag{5.3}$$

Equation 3.5 and 3.6 are both satisfied on every triangular faces. Let $\mu_f(T) = \rho_T + \sqrt{-1}\ \tau_T$. The discrete versions of Equation 3.5 and 3.6 can be obtained.

$$\begin{aligned} -d_T &= \alpha_1(T)a_T + \alpha_2(T)b_T \\ c_T &= \alpha_2(T)a_T + \alpha_3(T)b_T \end{aligned} \tag{5.4}$$

and

$$\begin{aligned} -b_T &= \alpha_1(T)c_T + \alpha_2(T)d_T \\ a_T &= \alpha_2(T)c_T + \alpha_3(T)d_T \end{aligned} \tag{5.5}$$

where: $\alpha_1(T) = \frac{(\rho_T-1)^2+\tau_T^2}{1-\rho_T^2-\tau_T^2}$; $\alpha_2(T) = -\frac{2\tau_T}{1-\rho_T^2-\tau_T^2}$; $\alpha_3(T) = \frac{1+2\rho_T+\rho_T^2+\tau_T^2}{1-\rho_T^2-\tau_T^2}$.

In order to discretize Equation 3.7, we need to introduce the *discrete divergence*. The discrete divergence can be defined as follows. Let $T = [v_i, v_j, v_k]$ and $w_I = f(v_I)$ where $I = i, j$ or k. Suppose $v_I = g_I + \sqrt{-1}\ h_I$ and $w_I = s_I + \sqrt{-1}\ t_I$ $(I = i, j, k)$. Using equation 5.2, a_T, b_T, c_T and d_T can be written as follows:

$$\begin{aligned} a_T = A_i^T s_i + A_j^T s_j + A_k^T s_k;\ b_T = B_i^T s_i + B_j^T s_j + B_k^T s_k; \\ c_T = A_i^T t_i + A_j^T t_j + A_k^T t_k;\ d_T = B_i^T t_i + B_j^T t_j + B_k^T t_k; \end{aligned} \tag{5.6}$$

where:

$$\begin{aligned} A_i^T = (h_j - h_k)/Area(T),\ A_j^T = (h_k - h_i)/Area(T),\ A_k^T = (h_i - h_j)/Area(T); \\ B_i^T = (g_k - g_j)/Area(T),\ B_j^T = (g_i - g_k)/Area(T),\ B_k^T = (g_j - g_i)/Area(T); \end{aligned} \tag{5.7}$$

Suppose $\vec{V} = (V_1, V_2)$ is a discrete vector field defined on every triangular faces. For each vertex v_i, let N_i be the collection of neighborhood faces attached to v_i. We define the discrete divergence Div of $\vec{V}$ as follows:

$$Div(\vec{V})(v_i) = \sum_{T \in N_i} A_i^T V_1(T) + B_i^T V_2(T) \tag{5.8}$$

By careful checking, one can prove that

$$\sum_{T \in N_i} A_i^T b_T = \sum_{T \in N_i} B_i^T a_T;\ \sum_{T \in N_i} A_i^T d_T = \sum_{T \in N_i} B_i^T c_T. \tag{5.9}$$

This gives,

$$Div \begin{pmatrix} -D_y u \\ D_x u \end{pmatrix} = 0 \ \text{ and } \ Div \begin{pmatrix} -D_y v \\ D_x v \end{pmatrix} = 0 \tag{5.10}$$

As a result, Equation (3.7) can be discretized:

$$Div \left(A \begin{pmatrix} D_x u \\ D_y u \end{pmatrix} \right) = 0 \ \text{ and } \ Div \left(A \begin{pmatrix} D_x v \\ D_y v \end{pmatrix} \right) = 0 \tag{5.11}$$

where $A = \begin{pmatrix} \alpha_1 & \alpha_2 \\ \alpha_2 & \alpha_3 \end{pmatrix}$. This is equivalent to:

$$\sum_{T \in N_i} A_i^T [\alpha_1(T) a_T + \alpha_2(T) b_T] + B_i^T [\alpha_2(T) a_T + \alpha_3(T) b_T] = 0 \tag{5.12}$$

$$\sum_{T \in N_i} A_i^T [\alpha_1(T) c_T + \alpha_2(T) d_T] + B_i^T [\alpha_2(T) c_T + \alpha_3(T) d_T] = 0 \tag{5.13}$$

for all vertices $v_i \in D$. Note that a_T and b_T can be written as a linear combination of the x-coordinates of the desired quasi-conformal map f. Hence, equation 5.12 gives us the linear systems to solve for the x-coordinate function of f. Similarly, c_T and d_T can also be written as a linear combination of the y-coordinates of the desired

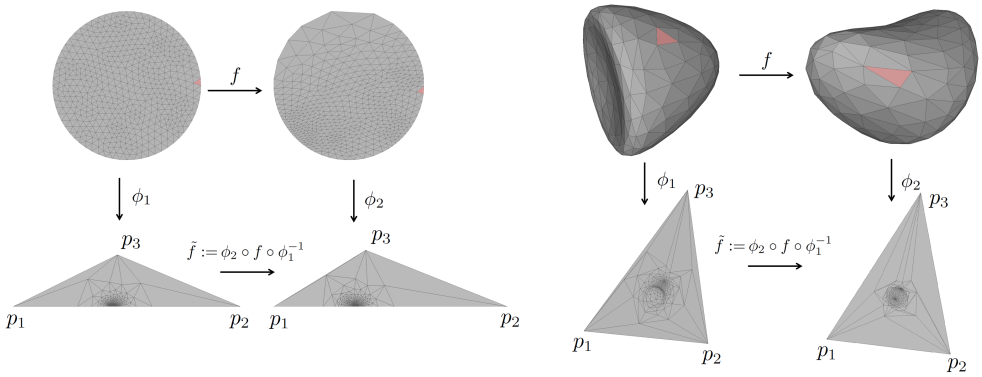

FIG. 5.1. *Illustration of how quasiconformal mapping between surface meshes can be transformed to a quasiconformal mapping between big triangles in* $\mathbb{R}^2$. *(A) shows a quasiconformal mapping between unit disks (or simply-connected open meshes of disk topology). The two meshes are conformally mapped to a big triangle after cutting a triangular face near 1. Through composition, the quasiconformal mapping can be transformed to a quasiconformal mapping between the big triangles in* $\mathbb{R}^2$. *(B) shows the case of a homeomorphism between genus-0 closed surface meshes. The two meshes are conformally parameterized onto a big triangle in* $\mathbb{R}^2$, *after cutting away a triangular face on each mesh. Again, through composition, the quasiconformal mapping can be transformed to a quasiconformal mapping between the big triangles in* $\mathbb{R}^2$.

quasi-conformal map f. Therefore, equation 5.13 gives us the linear systems to solve for the y-coordinate function of f.

Besides, f has to satisfy certain constraints on the boundary. One common situation is to give the Dirichlet condition on the whole boundary. That is, for any $v_b \in \partial K_1$

$$f(v_b) = w_b \in \partial K_2 \tag{5.14}$$

Note that the Dirichlet condition is not required to be enforced on the whole boundary. The proposed algorithm also allows free boundary condition. In the case that K_1 and K_2 are rectangles, the desired quasi-conformal map should satisfy

$$\begin{aligned} f(0) = 0; f(1) = 1\ f(i) = i\ f(1+i) = 1+i; \\ \mathbf{Re}(f) = 0 \text{ on arc } [0,i];\ \mathbf{Re}(f) = 1 \text{ on arc } [1,1+i]; \\ \mathbf{Imag}(f) = 0 \text{ on arc } [0,1];\ \mathbf{Imag}(f) = 1 \text{ on arc } [i,1+i] \end{aligned} \tag{5.15}$$

When K_i $(i = 1, 2)$ is an unit disk, we can parameterize it onto a domain D_i, which is a triangle with boundary vertices p_0^i, p_1^i and p_2^i. p_0^i is on the y-axis whereas p_1^i and p_2^i are on the x-axis. This can be done by removing a triangular face at the point 1 and map K_i to the upper half plane using a Mobiüs transformation: $\psi(z) = \sqrt{-1}\frac{1+z}{1-z}$ (See Figure 5.1). In this case, the desired quasi-conformal map f should satisfy

$$f(p_0^1) = p_0^2; f(p_1^1) = p_1^2 \ \text{ and } \ \mathbf{Imag}(f) = 0 \text{ on arc } [p_0^1, p_1^1]; \tag{5.16}$$

When K_i $(i = 1, 2)$ is a genus-0 closed surface mesh, we can again parameterize it onto a domain D_i, which is a triangle with boundary vertices p_0^i, p_1^i and p_2^i. This can be done by removing a triangular face at the north pole and map K_i to the

2D plane using stereographic projection (See Figure 5.1). In this case, the desired quasi-conformal map f should satisfy

$$f(p_0^1) = p_0^2; f(p_1^1) = p_1^2 \text{ and } f(p_2^1) = p_2^2 \tag{5.17}$$

Suppose interior landmark correspondences $\{p_i\}_{i=1}^n \leftrightarrow \{q_i\}_{i=1}^n$ are also enforced, one should add this constraint to the linear system. Mathematically, it is described as $f(p_i) = q_i$ $(i = 1, 2, ..., n)$.

Equations 5.12 and 5.13 together with the above boundary conditions give a non-singular linear system to solve for f. The linear system is symmetric positive definite. Hence, it can be solved effectively by the conjugate gradient method. We call this algorithm the *Linear Beltrami Solver*(LBS). Given a Beltrami coefficient ν, we denote the obtained quasi-conformal map from LBS by **LBS**(ν). If landmark constraints are enforced, we denote it by $\mathbf{LBS}_{LM}(\nu)$.

We note that given an arbitrary Beltrami coefficient ν and arbitrary landmark correspondences, a quasi-conformal mapping associated to ν might not exist. However, the Linear Beltrami Solver looks for the best quasi-conformal mapping whose Beltrami coefficient closely resemble to ν.

5.2. Quasi-conformal(QC) iterations. With the Linear Beltrami Solver, one can easily obtain the best quasi-conformal mapping associated with a given BC. In order to obtain the T-Map f, our goal is to iteratively search for the optimal BC associated to f. With the optimal BC, the desired T-Map f can be easily reconstructed using the Linear Beltrami Solver.

Recall that our problem of computing the T-Map can be formulated into an optimization problem:

$$(\nu, f) = \mathbf{argmin}_{\nu: D_1 \to \mathbb{C}}\{||\nu||_\infty\} \tag{5.18}$$

subject to: (1) $\nu = \mu(f)$ with $||\nu||_\infty < 1$; (2) $\nu = k\frac{\overline{\varphi}}{\varphi}$ for some constant k and holomorphic function $\varphi : D_1 \to \mathbb{C}$; and (3) f satisfies certain boundary condition and/or landmark constraints. Note that the boundary condition in (3) can either be a Dirichlet condition defined on the whole boundary or a free boundary condition with only few points on the boundary fixed. In this subsection, we introduce the *Quasi-conformal(QC) iteration* to solve the above optimization problem.

The QC iteration starts with an initial map $f_0 : D_1 \to D_2$ satisfying the given boundary condition and landmark constraints. The initial map is chosen to be the quasi-conformal mapping obtained from LBS associated to the initial BC $\mu_0 = 0$. In other words,

$$f_0 = \mathbf{LBS}_{LM}(\mu_0 := 0) \tag{5.19}$$

Note that with the enforced landmark constraints, the Beltrami coefficient associated to f_0 might not be equal to $\mu_0 = 0$. The Linear Beltrami Solver simply look for the best quasi-conformal mapping whose Beltrami coefficient resemble to μ_0 as much as possible. Let ν_0 be the actual Beltrami coefficient associated to f_0. This gives us a pair (f_0, ν_0), for which $\nu_0 = \mu(f_0)$.

Now, in order to minimize the energy function E_2 satisfying condition (2), we propose to perform a Laplace smooth $\mathfrak{L}$ and averaging $\mathfrak{A}$ on ν_0. The Laplace smooth $\mathfrak{L}$, which aims to minimize E_2, is given by the following:

$$\mathfrak{L}(\nu_0)(T) := \sum_{T_i \in \text{Nbhd}(T)} \nu_0(T) \ /|\text{Nbhd}(T)| \tag{5.20}$$

where T is a triangular face of K_1, Nbhd(T) is the set of neighborhood faces of T and $|\text{Nbhd}(T)|$ is the number of neighborhood faces in the set Nbhd(T). Set $\tilde{\mu_1}(T) = \mathfrak{L}(\nu_0)(T)$.

The averaging operator $\mathcal{A}$ is defined as follows:

$$\mu_1(T) = \mathcal{A}(\tilde{\mu_1})(T) := \left(\frac{\sum_{T\in \text{ all faces of } K_1} |\tilde{\mu_1}|(T)}{\text{No. of faces of } K_1}\right)\frac{\tilde{\mu_1}(T)}{|\tilde{\mu_1}(T)|} \tag{5.21}$$

$\mathcal{A}$ aims to obtain an optimal ν satisfying the condition (2) in the optimization problem. An updated quasi-conformal, f_1 can then be obtained by LBS: $f_1 = \mathbf{LBS}_{LM}(\mu_1)$. And an updated Beltrami coefficient, $\nu_1 := \mu(f_1)$, can be computed. Thus, we get a new pair (f_1, ν_1).

The procedure continues until the iteration converges. More specifically, given the pair (f_n, ν_n) obtained at the n iteration, we can obtain a new pair (f_{n+1}, ν_{n+1}) as follows:

$$\begin{aligned} &\mu_{n+1} := \mathcal{A}(\mathfrak{L}(\nu_n)); \\ &f_{n+1} := \mathbf{LBS}_{LM}(\mu_{n+1}); \\ &\nu_{n+1} := \mu(f_{n+1}). \end{aligned} \tag{5.22}$$

Consequently, we get a sequence of pair (f_n, ν_n), which converges to the optimal Beltrami coefficient associated to the T-Map. In practice, we stop the iteration when $||\nu_{n+1} - \nu_n|| < \epsilon$.

We summarize the QC iteration as follows.

Algorithm 5.1 : *(QC iteration for open surfaces)*
Input : *Triangular meshes: K_1 and K_2; the desired landmark constraints and/or boundary condition.*
Output : *Optimal Beltrami coefficient ν and the T-Map f*

1. *Obtain the initial mapping $f_0 = \mathbf{LBS}_{LM}(\mu_0 := 0)$. Set $\nu_0 = \mu(f_0)$;*
2. *Given ν_n, compute $\mu_{n+1} := \mathcal{A}(\mathfrak{L}(\nu_n))$; Compute $f_{n+1} := \mathbf{LBS}_{LM}(\mu_{n+1})$ and set $\nu_{n+1} := \mu(f_{n+1})$;*
3. *If $||\nu_{n+1} - \nu_n|| \geq \epsilon$, continue. Otherwise, stop the iteration.*

The QC iteration can also be applied to the case when D_i $(i = 1, 2)$ is a unit sphere. In other words, given a set of landmark constraints between the unit sphere, our goal is to look for the T-Map $f : D_1 \to D_2$. However, special attention has to be paid in this case.

Denote the landmark correspondence by $\{p_i\}_{i=1}^n \leftrightarrow \{q_i\}_{i=1}^n$. We can assume that the north pole is fixed. If not, it can also be achieved by a Mobiüs transformation. The LBS can be applied to unit spheres, by stereographically projecting D_i onto a big triangles in $\mathbb{R}^2$ (See Figure 5.1). However, numerical error near the north pole is inevitable. We therefore propose an alternating scheme to fix this problem.

For the initial map, we add the vertices near the north pole $\{n_j\}_{j=1}^m$ $(z > 0.99)$ as landmarks and fix all $\{n_j\}_{j=1}^m$. We then compute the T-Map f_0 using Algorithm 5.1. Numerical error will be introduced near the north pole. To fix it, in our next step, we consider the vertices $\{s_j\}_{j=1}^m$ near the south pole $(z < -0.99)$ as landmarks. The correspondence is given by: $s_j \leftrightarrow f_1(s_j)$. Rotate the south pole of D_i to the north pole by a Mobiüs transformation. We can again compute the T-Map f_2 using Algorithm 5.1.

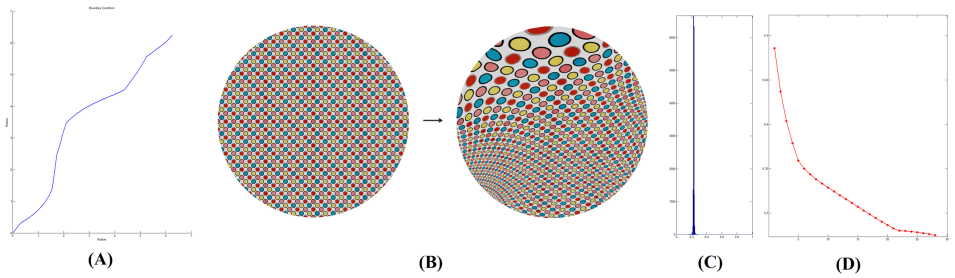

FIG. 5.2. *Example of the T-Map of the disk with fixed Dirichlet boundary condition. (A) shows the boundary condition. (B) shows the obtained T-Map, visualized using the texture mapping. (C) shows the histogram of the BC norm. (D) shows the sup-norm of the BC in each QC iterations.*

We continue this process until the iteration converges. More specifically, at the n iteration where n is an even integer, we add vertices $\{s_j\}_{j=1}^m$ around south pole as landmarks. Set correspondence as: $s_j \leftrightarrow f_n(s_j)$. Rotate the south pole of D_i to the north pole by a Mobiüs transformation, and obtain the T-Map f_{n+1} using Algorithm 5.1. When n is an odd integer, we add vertices $\{n_j\}_{j=1}^m$ around north pole as landmarks. Set correspondence as: $n_j \leftrightarrow f_n(n_j)$ and obtain the T-Map f_{n+1} using Algorithm 5.1. Set $\nu_{n+1} = \mu(f_n)$.

This alternating process between the north pole and the south pole continues until $||\nu_{n+1} - \nu_n|| < \epsilon$.

The detailed algorithm can be summarized as follows:

Algorithm 5.2 : *(QC iteration for genus-0 closed surfaces)*
Input : *Triangular meshes: K_1 and K_2; the desired landmark constraints and/or boundary condition.*
Output : *Optimal Beltrami coefficient ν and the T-Map f*

1. *Add vertices around north pole as landmarks and fix their positions. Obtain the initial T-Map f_0 using Algorithm 5.1. Set $\nu_0 = \mu(f_0)$;*
2. *Given f_n and ν_n. When n is even, add vertices $\{s_j\}_{j=1}^m$ around south pole as landmarks. Set correspondence as: $s_j \leftrightarrow f_n(s_j)$. Rotate the south pole of D_i to the north pole. When n is odd, add vertices $\{s_j\}_{j=1}^m$ around south pole as landmarks. Set correspondence as: $s_j \leftrightarrow f_n(s_j)$. Obtain the T-Map f_{n+1} using Algorithm 5.1. Set $\nu_{n+1} = \mu(f_n)$;*
3. *If $||\nu_{n+1} - \nu_n|| \geq \epsilon$, continue. Otherwise, stop the iteration.*

When D_i $(i = 1, 2)$ is a unit disk, the LBS would also introduce numerical error near 1. To fix it, the same alternating algorithm between 1 and -1 can be applied.

The QC iterations can also be extended to compute T-Map with soft landmark constraints. It will become useful when landmark features cannot be accurately located, and hence it is better to compute registration with landmarks approximately (but not exactly) matched. Denote the landmark correspondence by $\{p_i\}_{i=1}^n \leftrightarrow \{q_i\}_{i=1}^n$. Instead of enforcing a hard landmark constraints, a soft constraints can be introduced by requiring $||p_i - q_i|| < \delta$ for all $i = 1, 2, ..., n$. This can be done easily by firstly computing a rough guess of a landmark matching T-Map g using Algorithm 5.1 or 5.2. The BC, μ_g, of g can be computed. Starting with μ_g, Algorithm 5.1 or 5.2 can be applied to compute a T-Map without enforcing the

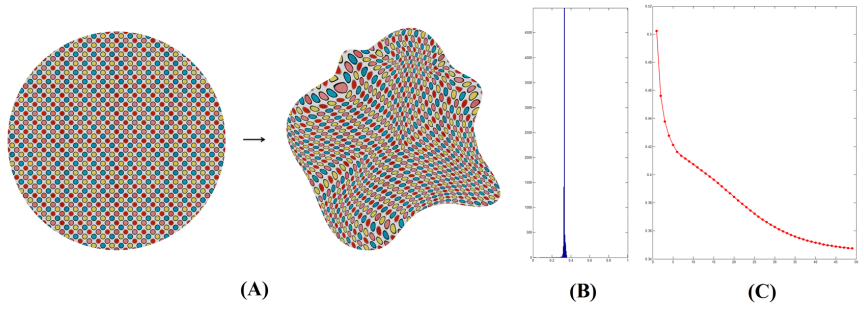

FIG. 5.3. *Another example of the T-Map of the disk with fixed Dirichlet boundary condition. (A) shows the obtained T-Map, visualized using the texture mapping. (B) shows the histogram of the norm of the BC. (C) shows the sup-norm of the BC in each QC iterations.*

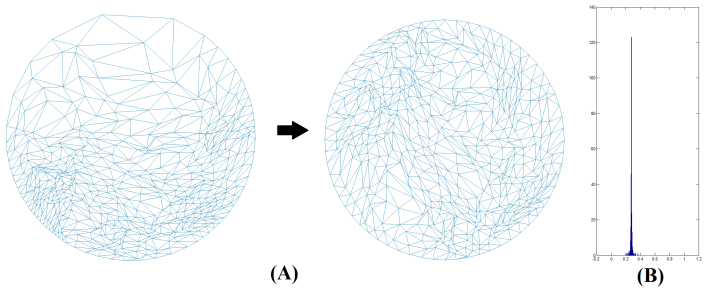

FIG. 5.4. *Computation of T-Map on an irregular mesh. The QC iteration is independent of the mesh structure. The boundary condition is given and the associated T-Map is constructed, as shown in (A). (B) shows the right shows the histogram of the norm of the BC.*

interior landmark constraints. A T-Map with soft landmark constraints can then be obtained. The detailed algorithm can be described as follows:

Algorithm 5.3 : *(QC iteration for soft landmark constraints)*
Input : *Triangular meshes: K_1 and K_2; desired landmark constraints and/or boundary condition; landmark constraint tolerance δ*
Output : *Optimal Beltrami coefficient ν and the T-Map f*

1. *Obtain an initial guess of landmark matching T-Map g_0 using Algorithm 5.1 or 5.2. Set the stopping criteria to be $||\nu_{n+1} - \nu_n|| < 100\epsilon$.*
2. *Given g_n and $\mu_n = BC$ of g_n. Starting from μ_n, compute the T-Map g_{n+1} using Algorithm 5.1 or 5.2, without setting the interior landmark constraints. Set the stopping criteria to be $||\nu_{n+1} - \nu_n|| < \epsilon$. Let $\mu_{n+1} = BC$ of g_{n+1}.*
3. *If $||p_i - q_i|| \geq \delta$ for some $i = 1, 2, ..., n$, continue. Otherwise, stop the iteration.*

6. Numerical experiments. In this section, we evaluate our proposed algorithm numerically by synthetic examples.

6.1. T-Map of simply-connected domains. In our first numerical experiment, we test our method to compute the T-Map of the unit disk with a given Dirichlet boundary condition. A Dirchlet condition on the whole boundary is given as shown in

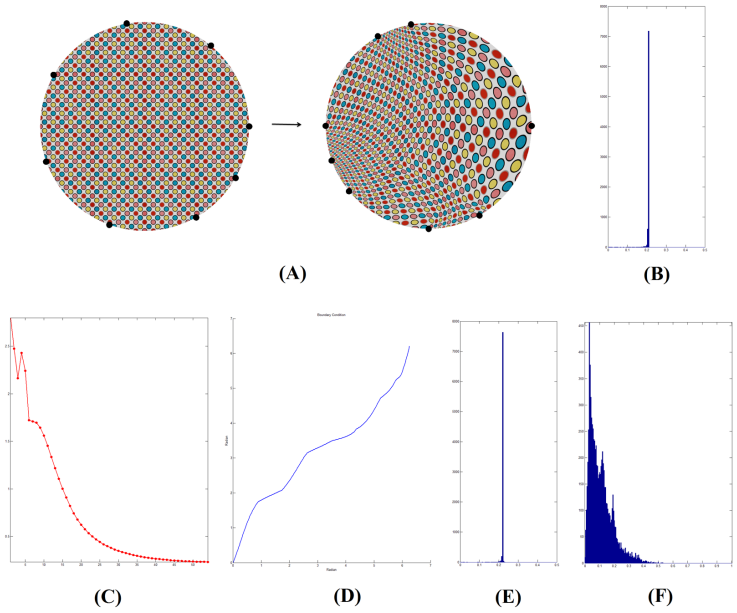

FIG. 5.5. *T-Map of the disk with only 8 landmark points constraints on the boundary. (A) shows the T-Map. (B) shows the histogram of the BC norm. (C) shows the sup-norm of the BC in each QC iteration. (D) shows the automatically obtained optimal boundary correspondence. (E) shows the histogram of the BC norm under the T-Map with arc-length parameterized boundary condition. (F) shows the histogram of the BC norm under harmonic map with arc-length parameterized boundary condition.*

Figure 5.2(A). The obtained T-Map is shown in (B), which is visualized using the texture mapping. Note that the original texture is deformed under the T-Map. However, the dilations of the ellipses deformed from the small circles are the same. It means the norm of the BC is constant everywhere. The histogram of the norm of the BC is also shown in (C), which again demonstrates the norm of the BC is equal to a constant $k = 0.15016$. The standard deviation of the BC norm is 0.0034373. Under the QC iteration, we iteratively obtain a sequence of pair $\{f_n, \nu_n = \mu(f_n)\}_{n=0}^{\infty}$. (D) shows the supreme norm of BC, $||\nu_n||_\infty$, in each QC iterations. It decreases as iteration increases, indicating that the algorithm converges to an optimized T-Map minimizing the maximal conformality distortion. Also, the algorithm converges quickly in less than 20 iterations.

Besides, the Dirichlet boundary condition can be of arbitrary shapes. Figure 5.3 shows a T-Map between the unit disk and the ameba shape with given boundary conditions. The norm of BC is also constant everywhere, as demonstrated in (B), indicating that the obtained mapping is indeed a T-Map. (C) shows the sup-norm of BC in each QC iterations.

Our proposed QC iteration is also independent of the mesh structure. Figure 5.4(A) shows a mesh with an irregular mesh structure. The boundary condition is given and the associated T-Map is constructed. (B) shows the histogram of the norm of the BC, which is accumulated at 0.28. It demonstrates the obtained map is indeed a T-Map. This result shows that our proposed method is effective for computing a

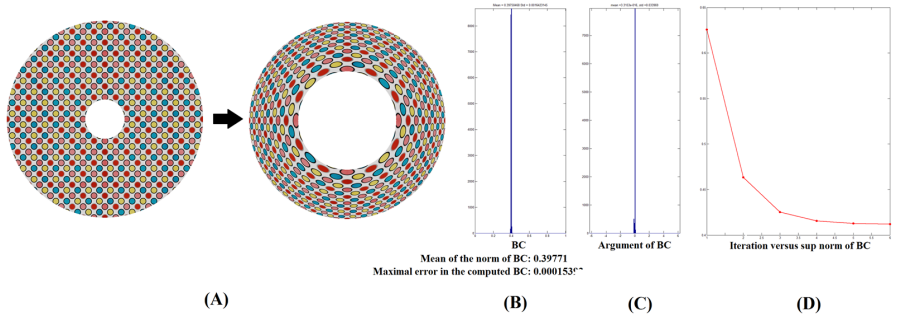

FIG. 6.1. *T-Map of the annulus with fixed Dirichlet boundary condition. (A) shows the obtained T-Map, visualized using the texture mapping. (B) shows the histogram of the BC norm. (C) shows the histogram of the Laplacian of the argument of the BC. (D) shows the sup-norm of the BC in each QC iterations.*

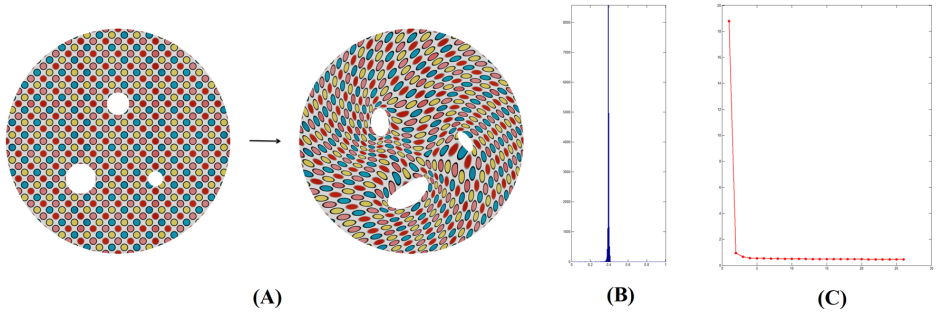

FIG. 6.2. *T-Map of the multiply-connected domain containing three holes with fixed Dirichlet boundary condition. (A) shows the obtained T-Map. (B) shows the histogram of the norm of the BC. (C) shows the sup-norm of the BC in each QC iterations.*

bijective T-Map between meshes, even with irregular mesh structure.

Our algorithm can also be applied to the situation when only a few landmark constraints are enforced on the boundary (instead of the Dirichlet condition defined on the whole boundary). In Figure 5.5, we test our algorithm to compute the T-Map of the unit disk with only 8 landmark points constraints on the boundary. (A) shows the the T-Map. Again, the dilations of the ellipses deformed from the small circles are the same, meaning that the norm of the BC is constant everywhere. (B) shows the histogram of the BC norm. The norm k of the BC is equal to 0.201. (C) shows the sup-norm of the BC in each QC iterations. Again, it converges quickly in less than 60 iterations. Our algorithm automatically detects the optimal boundary correspondence. (D) shows the obtained optimal boundary correspondence. (E) shows the histogram of the BC norm under the T-Map with arc-length parameterized boundary condition (of which the prescribed constraints on the boundary are satisfied). Although a T-Map can still be obtained, the norm of the BC is equal to 0.23 which is higher than the case when only 8 points landmark constraints are enforced. Hence, the obtained T-Map is not extremal. (F) shows the histogram of the BC norm under the harmonic map with arc-length correspondence on the boundary. Note that the

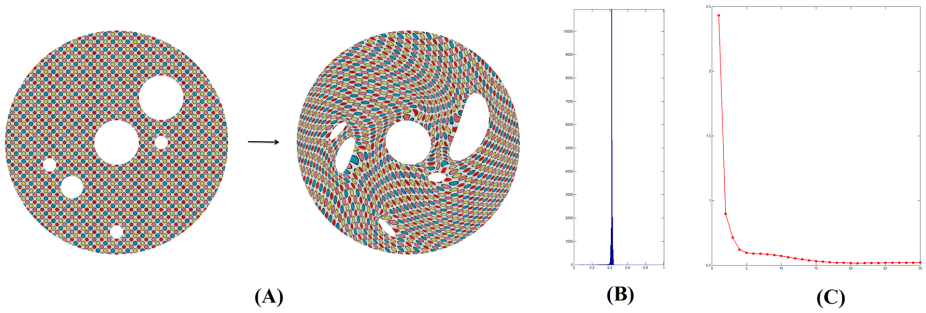

FIG. 6.3. *T-Map of the multiply-connected domain containing six holes with fixed Dirichlet boundary condition. (A) shows the obtained T-Map. (B) shows the histogram of the norm of the BC. (C) shows the sup-norm of the BC in each QC iterations.*

distribution of the conformality distortion is highly non-uniform.

6.2. T-Map of multiply-connected domains. Our method can also be applied to multiply-connected domains. In Figure 6.1, we test our method to compute the T-Map of an annulus with Dirichlet boundary condition. (A) shows the obtained T-Map. (B) shows the histogram of the norm of BC, which illustrates the obtained map is indeed an T-Map. Besides, the BC of a T-Map is of the form: $\mu = k\frac{\overline{\varphi}}{\varphi}$, where φ is holomorphic. The imaginary part of $\log(\mu)$, which is equal to the argument of μ, must be harmonic. (C) shows the Laplacian of the argument of the BC. It is accumulated at 0, meaning that the argument of the BC is indeed harmonic. (D) shows the supreme norm of the BC in each iterations. Again, it decreases as iteration increases and converges fastly in just 6 iterations.

In Figure 6.2, we compute the T-Map between multiply-connected domains having 3 holes with a given boundary condition. (A) shows the obtained T-Map. The histogram of the BC norm and the supreme norm of BC in each iterations are shown in (B) and (C) respectively. Note that the algorithm converges quickly in 10 iterations. Figure 6.3 demonstrates the result of T-Map between more complicated multiply-connected domains having 6 holes. The obtained T-Map is shown in (A). (B) and (C) show the histogram of the BC norm and the supreme norm of the BC in each iterations respectively. Again, the algorithm converges quickly in 30 iterations.

6.3. T-Map with interior landmark constraints. Our algorithm can compute the T-Map with interior landmark constraints enforced. Figure 6.4 shows the T-Map between the unit disk with 24 interior landmark constraints and few point constraints on the boundary enforced. (A) shows the 24 landmark constraints and 4 point constraints on the boundary. (B) shows the obtained T-Map, visualized using the texture mapping. (C) shows the sup-norm of the BC in each QC iterations, which converges within 30 iterations. (D) shows the histogram of the norm of the BC. The norm of the BC is uniformly equal to 0.2. (E) shows the histogram of the BC norm of a T-Map with the arc-length boundary correspondence enforced (of which the prescribed 4 points constraints on the boundary are satisfied). As expected, the norm of the BC is larger (=0.28), which means the T-Map is not an extremal one.

Besides, interior landmark curve constraints can be enforced. In Figure 6.5 , we test our algorithm to compute the T-Map of the unit disk with 3 interior landmark curve constraints enforced. (A) shows the obtained T-Map. (B) shows the histogram

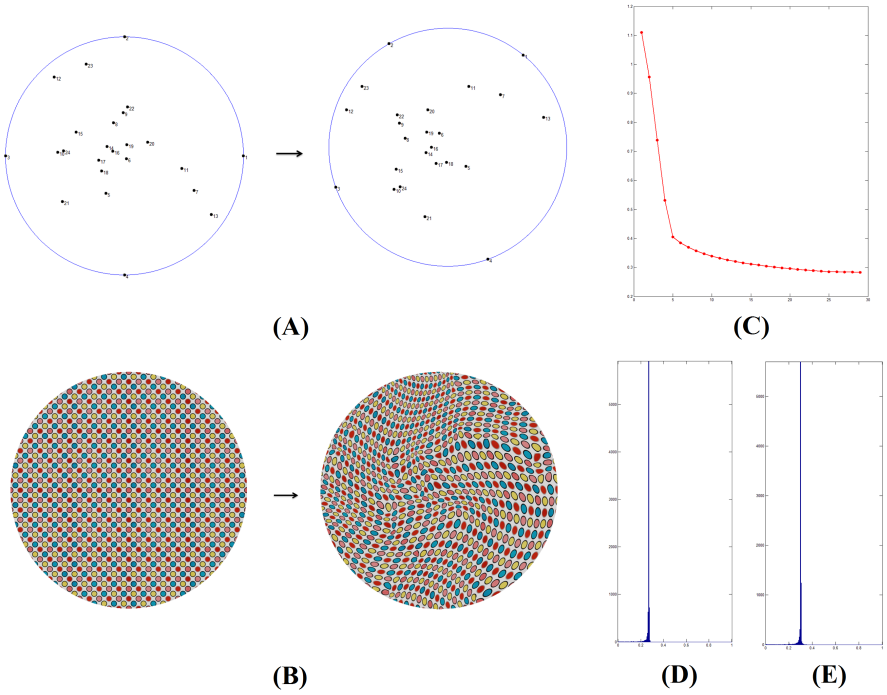

FIG. 6.4. *T-Map between the disks with 24 interior landmark constraints and 4 point constraints on the boundary enforced. (A) shows the 24 landmark constraints and 4 point constraints on the boundary. (B) shows the T-Map. (C) shows the sup-norm of the BC in each QC iterations. (D) shows the histogram of the norm of the BC. (E) shows the histogram of the BC norm under the T-Map with arc-length parameterized boundary condition.*

of the norm of the BC. The norm of the BC is accumulated at 0.53. (C) shows the sup-norm of the BC in each QC iterations. The sup-norm of the BC is decreasing, indicating that the algorithm converges to an optimized T-Map, minimizing the maximal conformality distortion.

We also test our algorithm for the case when only interior landmark constraints are enforced (without boundary condition). Figure 6.6 shows the computed T-Map with 20 interior landmark point constraints enforced. (A) shows the constraints of the feature points. (B) shows the obtained T-Map. (C) shows the histogram of the norm of the BC. Although no boundary constraint is enforced, our algorithm is able to automatically determine an optimal boundary correspondence of the T-Map minimizing the geometric distortion.

Besides the hard landmark constraints, our algorithm can also be applied to compute T-Map with soft landmark constraints. Figure 6.7 shows an example of T-Map of the unit disk with soft landmark constraints. (A) shows the T-Map with hard landmark constraints enforced. The histogram of the norm of BC is plotted, which is accumulated at 0.41. Landmarks are perfectly matched. (B) shows the obtained T-Map with soft landmark constraints. Landmarks cannot be exactly matched, but less conformality distortion is introduced. As shown in the histogram of the BC, the norm of BC is accumulated at 0.35. It is less than that of the case when hard landmark constraints are enforced.

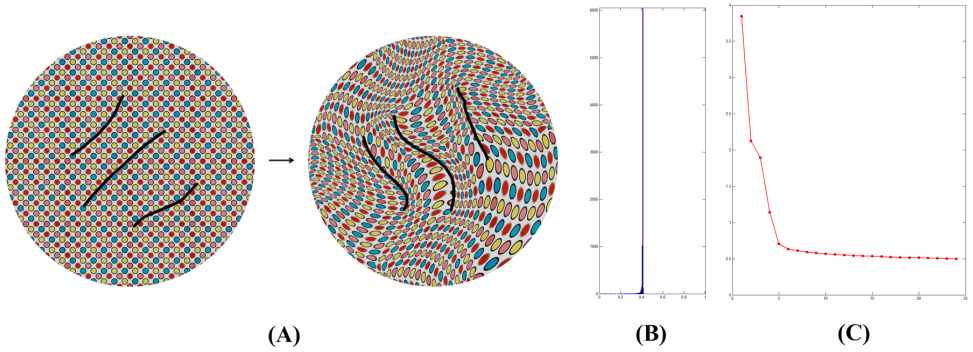

FIG. 6.5. *T-Map between the disks with 3 interior landmark curves constraints enforced. (A) shows the T-Map with 3 landmark curves constraints enforced. (B) shows the histogram of the norm of the BC. (C) shows the sup-norm of the BC in each QC iterations.*

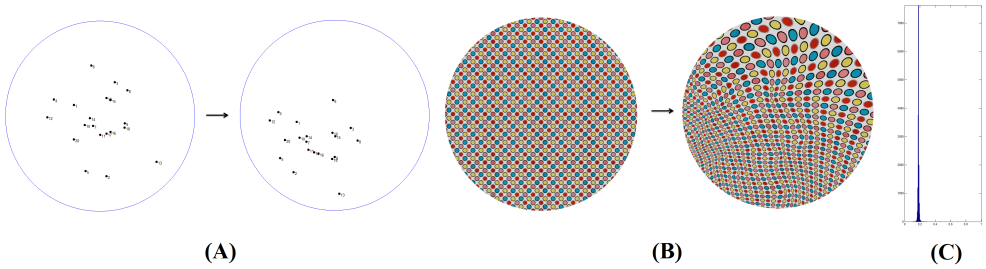

FIG. 6.6. *T-Map between the unit disks with 20 interior landmark constraints enforced (without boundary constraints). (A) shows the 20 landmark constraints. (B) shows the T-Map. (C) shows the histogram of the norm of the BC.*

Our algorithm can as well be applied to computing the T-Map between the unit sphere with interior landmark constraints enforced. Figure 6.8(A) shows 20 landmark constraints on the sphere. (B) shows the obtained T-Map. (C) shows the histogram of the norm of the BC. The norm of the BC is concentrated near 0.21, meaning that the mapping is indeed a T-Map.

6.4. Computational time. To test the efficiency of the QC iterations, we record the computational time of the proposed QC iterations. All our experiments were done on a laptop with an Intel Core i7 2.70 GHz CPU and 8 GB RAM. In Table 6.1, we list the computational time of the QC iterations for the experiments we have done. Note that for reasonably dense mesh ($\sim$ 8K vertices), the computational time is generally less than 10 seconds. For more complicated domains with denser meshes, the computational time is longer but the whole computation can still be done within 35 seconds. We note that the implementation of the QC iterations has not been optimized. It is currently implemented using Matlab. The implementation of the algorithm can be further improved. Also, the algorithm can be parallelized. Using GPU, it is believed that the computational time can be dramatically speeded up.

6.5. Comparison with existing methods. To test the effectiveness of our proposed method, we compare our algorithm with other existing methods. In Figure 6.9, we compare the landmark matching T-Map with three other exisiting methods,

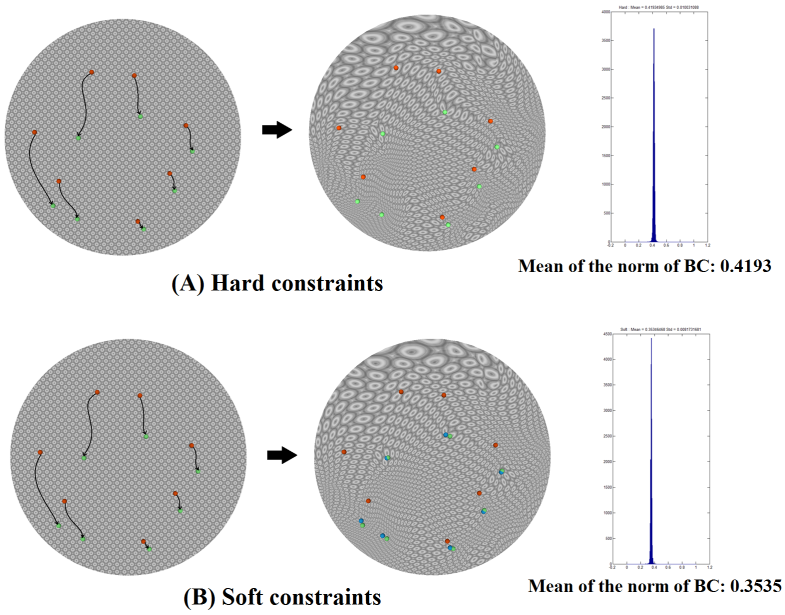

FIG. 6.7. *T-Map with soft landmark constraints. (A) shows the obtained T-Map with hard landmark constraints. The histogram of the norm of BC is plotted, which is accumulated at 0.4193. (B) shows the obtained T-Map with soft landmark constraints. Landmarks cannot be exactly matched, but less conformality is introduced, as shown in the histogram of the norm of the BC.*

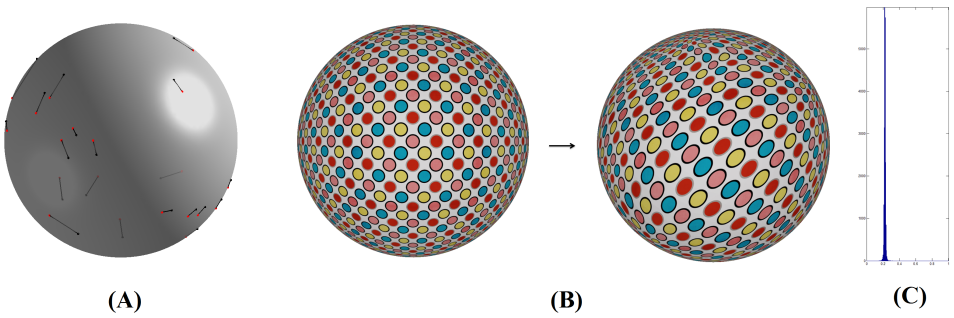

FIG. 6.8. *T-Map between the spheres. (A) shows landmark constraints on the sphere. (B) shows the T-Map. (C) shows the histogram of the norm of the BC.*

namely, 1. the harmonic map [20]; 2. thin plate spline (TPS) [19] and 3. LDDMM [10, 11, 12, 13, 14]. Seven landmark correspondences are enforced, as shown in (A). (B) shows the obtained landmark matching T-Map. It is bijective and landmarks are perfectly matched. (C) shows the landmark matching harmonic map. Landmarks are exactly matched, but overlaps (flips) occur. (D) shows the mapping obtained from TPS. Landmarks are not exactly matched and overlaps occur. (E) shows the mapping obtained from LDDMM. A smooth bijective mapping can be obtained. Also, landmarks can be better matched (although not perfectly) .

Table 6.2 gives the quantitative comparison between different methods. Harmonic map and TPS are the fastest algorithms. However, both methods cannot obtain a bi-

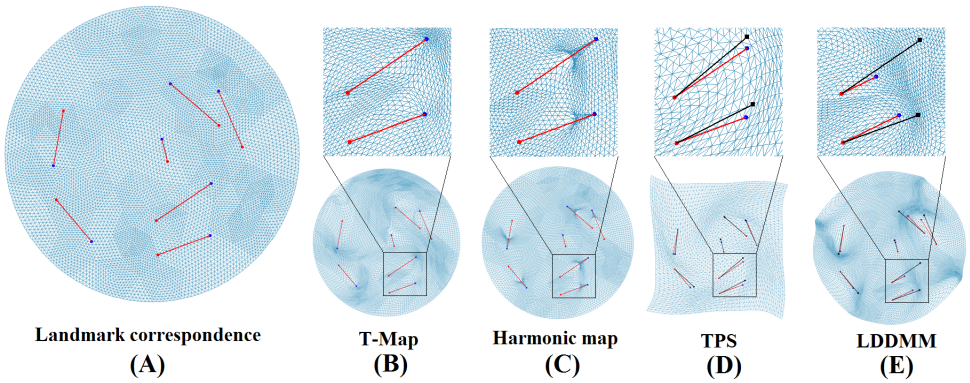

FIG. 6.9. *Comparison of the landmark matching T-Map with 1. the harmonic map; 2. thin plate spline (TPS) and 3. LDDMM. (A) shows 7 landmark point constraints. (B) shows the obtained landmark matching T-Map. (C) shows the landamrk matching harmonic map. (D)shows the mapping obtained from TPS. (E) shows the mapping obtained from LDDMM.*

TABLE 6.1
Computational time for QC iterations

	Vertex number	Time	$\|\|\mu\|\|_\infty$
Analytic example	8936	1.297 s	0.4122
4 points on boundary + 3 landmark curves	8257	4.46 s	0.4154
Disk (Dirichlet boundary)	8257	5.420 s	0.2295
8 points on boundary	8257	6.645 s	0.2120
4 points on boundary + 20 landmarks	8257	8.467 s	0.2843
Arbitrary shape	8257	10.056 s	0.3475
Disk free boundary + 20 landmarks	8257	18.579 s	0.1855
Three holes disk	17746	15.030 s	0.4088
Six holes disk	22979	17.680 s	0.4433
Sphere	10242	34.679 s	0.3086

jective mapping that matches landmark exactly. As a result, the sup-norm of the BC is big. It means that large conformality distortion is introduced. LDDMM can compute a smooth bijective mapping that closely matches landmarks. However, the computational cost is comparatively more expensive (416 seconds). Using our algorithm, we can obtain a bijective T-Map that matches landmarks perfectly. The conformality distortion, measured by the sup-norm of the BC, is also the smallest (=0.594). The computational time is also reasonably fast, which takes about 6 seconds.

7. Applications. In this section, we apply our proposed algorithms for computing landmark matching T-Maps to practical problems. More specifically, we will consider the problems of computing brain landmark matching registrations, constrained texture mappings and human face registrations.

7.1. Brain landmark matching registration. Landmark-based surface registrations are commonly applied for finding meaningful 1-1 correspondences between human brain cortical surfaces [20, 39, 21, 22, 23]. On cortical surfaces, sulcal landmarks can be labeled either manually by neuroscientists or automatically based on various geometric quantities [24]. The sulcal landmarks are important anatomical

TABLE 6.2
Comparison with other methods

	Teichmüller map	Harmonic map	TPS	LDDMM
Time	6.276 s	1.697s	0.117 s	416.247 s
Overlap faces	0	110	13	0
Landmark error	0	0	0.06126	0.24481
$\|\|\mu\|\|_\infty$	0.594	5.389	1	0.805

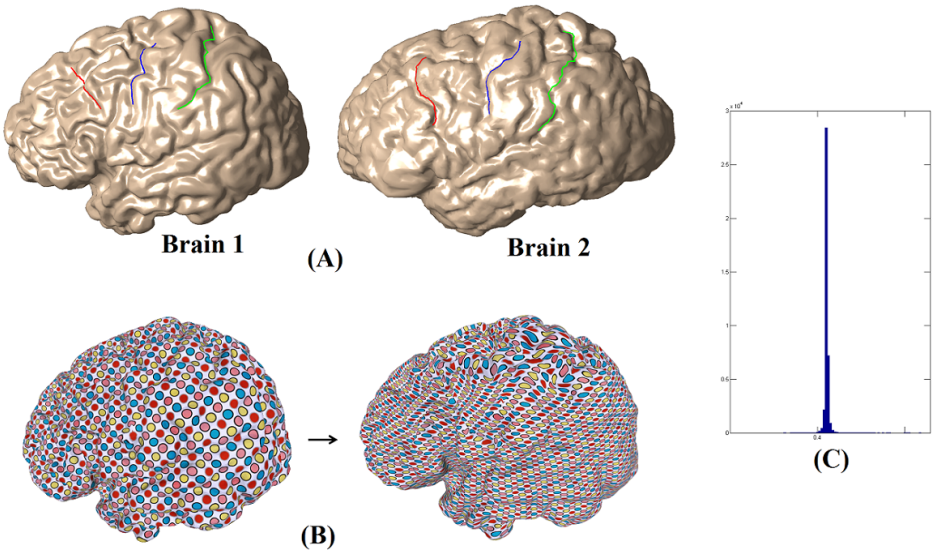

FIG. 7.1. *(A) shows 2 brain surfaces with 3 corresponding landmarks. (B) shows the T-Map with 3 landmark constraints enforced. (C) shows the histogram of the norm of BC.*

features. It is therefore desirable to obtain a registration between the cortical surfaces with least geometric distortion, which matches the sulcal landmarks as much as possible. Our algorithms for computing landmark matching T-Maps can be applied. In Figure 7.1, we apply our algorithm to compute the T-Map between 2 different brain surfaces with 3 corresponding landmarks labeled. (A) shows the corresponding sulcal landmarks, indicated by different colors. (B) shows the obtained T-Map with 3 landmark constraints enforced, visualized by the circle packing textures. The sulcal landmarks are exactly matched under the mapping. (C) shows the histogram of the norm of the associated BC. The norm is a constant showing that the obtained registration is indeed a T-Map. We also test the method to register cortical surfaces with more sulcal landmarks. In Figure 7.2, we compute the T-Map between 2 brain surfaces with 6 corresponding sulcal landmarks labeled. The obtained registration and the norm of its associated BC is shown in (B) and (C) respectively. The landmarks are exactly matched. Again, the norm of the BC is a constant, showing that the obtained registration is a T-Map which minimizes the conformality distortion.

7.2. Constrained texture mapping. Texture mapping is one of the major photorealistic techniques in computer graphics to generate realistic and visually rich 3D surfaces [32, 33]. It is usually done by putting each surface mesh in correspondence

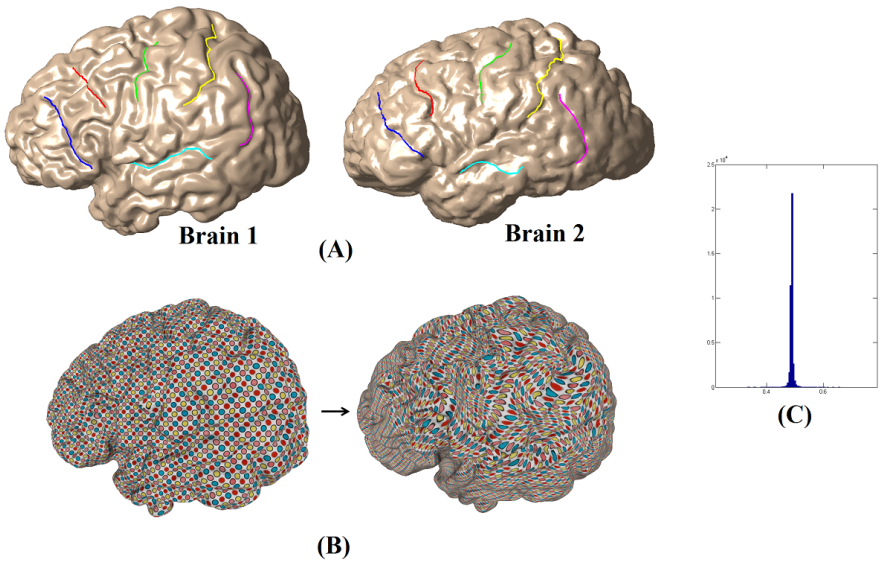

FIG. 7.2. *(A) shows 2 brain surfaces with 6 corresponding landmarks. (B) shows the T-Map with 6 landmark constraints enforced. (C) shows the histogram of the norm of BC.*

with a 2D image [2, 3, 37, 38, 36, 35, 34]. Such a correspondence between the surface mesh and the image is called the texture mapping. Constrained texture mappings are popularly used, in which the texture mappings are guided by landmark features labeled interactively by users. Ideally, the texture mapping should have minimum distortion, while matching the landmark points exactly. We apply our algorithms to compute the landmark matching T-Map between the surface mesh and the image, and use it as the texture mapping. In Figure 7.3, we map a cat image onto the human face surface. (A) shows the corresponding landmark points labeled manually on the human face and the texture image. The landmark matching T-Map is computed, and is used as texture mapping to project the cat image onto the human face. The textured surface is shown in (B). (C) shows the norm of the associated BC of the texture mapping. The norm is approximately a constant. It means the texture mapping computed is indeed a T-Map, which minimizes the conformality distortion.

In Figure 7.4, we further test our algorithm on a multiply-connected human face. (A) and (B) shows the texture(tiger) image and a multiply-connected human face. Corresponding landmark points are labeled manually on the texture image and the surface mesh. In (C), the surface mesh is mapped to a multiply-connected domain in 2D by a T-Map matching the landmark points exactly. (D) shows the textured surface. (E) shows the norm of the associated BC of the texture mapping. The norm is approximately a constant, which means the texture mapping computed is indeed a T-Map.

7.3. Human face registration. In face recognition, finding accurate spatial correspondences between human faces is an a crucial process to compare and recognize faces effectively [42, 40]. Corresponding features can be extracted on human face based on curvatures, such as high curvature points near nose tips and lips. Accurate face registration can then be obtained by computing a mapping that matches the corresponding features. Landmark matching T-Map, which minimizes the geometric

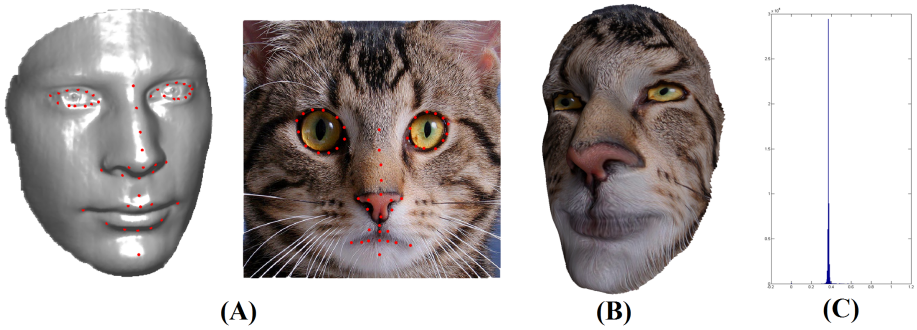

FIG. 7.3. *(A) shows a human face and a texture image of a cat. Corresponding landmark points are labeled on the surface and the texture image. We compute the T-Map that matches the landmark points. The T-Map is used as constrained texture mapping to project the texture image onto the surface, as shown in (B). (C) shows the histogram of the norm of BC.*

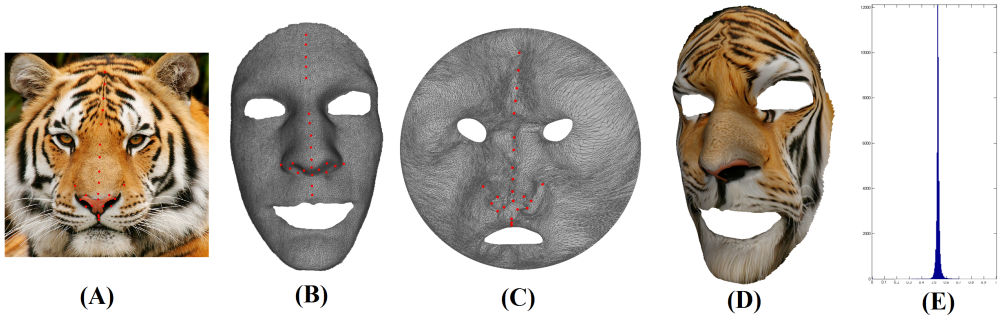

FIG. 7.4. *(A) a texture image of a tiger. (B) shows a multiply-connected human face. Corresponding landmark points are labeled on the surface and the texture image. In (C), the surface mesh is mapped to a multiply-connected domain in 2D by a T-Map matching the landmark points exactly. The T-Map is used as constrained texture mapping to project the texture image onto the surface, as shown in (D). (E) shows the histogram of the norm of BC.*

distortion, can then be used. In Figure 7.5, we apply our algorithm to compute the registration between a male and female human faces. The human faces are both simply-connected open surfaces. Corresponding feature points are labeled on both faces. The associated T-Map is obtained, which is visualized by texture mapping. The corresponding features are exactly matched. (C) shows the histogram of the norm of the BC, which is almost a constant. This demonstrates the obtained registration is a T-Map.

Our algorithm can also be applied to obtain registration between multiply-connected human faces. Figure 7.6 shows two multiply-connected human faces. Corresponding feature landmarks are labeled. T-Map matching the features exactly is computed, as shown in (B). It is again visualized by texture mapping. (C) shows the histogram of the norm of the BC. Again, it is almost a constant, which demonstrates that obtained registration is a T-Map minimizing the conformality distortion.

8. Conclusion. We address the problem of computing Teichmüller mappings (T-Maps) between surfaces, which minimizes the maximal conformality distortion. The proposed algorithm can be applied to obtain a landmark matching registration

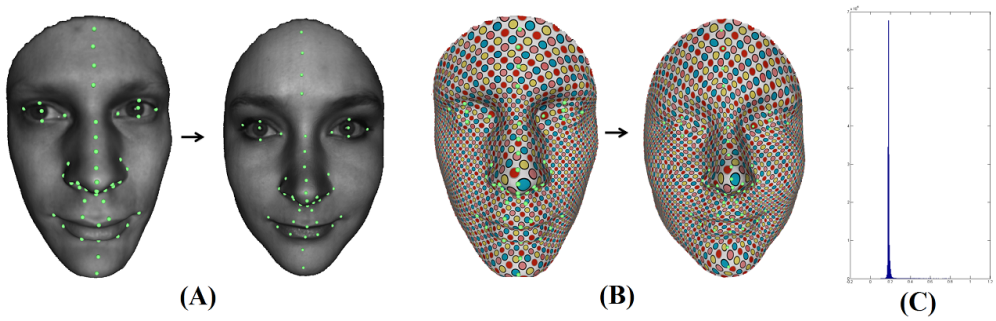

FIG. 7.5. *T-Map of the simply-connected domain with landmark point constraints (A) shows the two faces with landmark point constraints. (B) shows the T-Map of the two faces. The resultant mapping is illustrated by texture mapping. (C) shows the histogram of the norm of BC.*

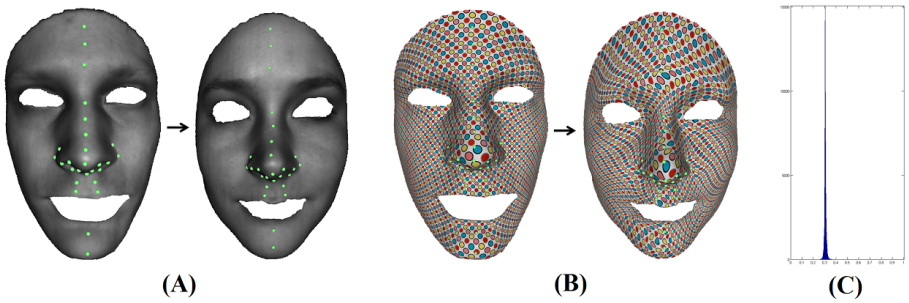

FIG. 7.6. *T-Map of the multiply-connected domain with landmark point constraints (A) shows the two faces with landmark point constraints. (B) shows the T-Map of the two faces. The resultant mapping is illustrated by texture mapping. (C) shows the histogram of the norm of BC.*

between surface meshes. Given a set of corresponding landmark points or curves defined on both surfaces, a unique landmark matching T-Map can be obtained, which minimizes the conformality distortion. In this paper, we propose an efficient iterative algorithm, called the Quasi-conformal (QC) iterations, to compute the T-Map. The key idea is to represent the set of diffeomorphisms by Beltrami coefficients (BCs). We then look for an optimal BC associated to the desired T-Map. The associated T-Map can be efficiently reconstructed from the optimal BC using the Linear Beltrami Solver(LBS). Using our proposed method, the T-Map between reasonably dense meshes can be accurately and efficiently computed. The obtained registration is guaranteed to be bijective. Besides, T-Map with soft landmark constraints can also be computed using our proposed algorithm. It becomes useful when landmark features cannot be accurately located, and hence it is better to compute registration with landmarks approximately (but not exactly) matched. We applied the proposed algorithm to real applications, such as brain landmark matching registration, constrained texture mapping and human face registration. Experimental results shows that our method is effective in computing a non-overlap landmark matching registration with least amount of conformality distortion.

REFERENCES

[1] B. Lévy, S. Petitjean, N. Ray and J. Maillot, *Least Squares Conformal Maps for Automatic Texture Atlas Generation*, ACM SIGGRAPH conference proceedings, 2002
[2] E. Zhang, K. Mischaikow and G. Turk, *Feature-based surface parameterization and texture mapping*, ACM Transactions on Graphics (TOG), Volume 24 Issue 1, January 2005
[3] S. Haker, S. Angenent, A. Tannenbaum, R. Kikinis, G. Sapiro, and M. Halle. *Conformal surface parameterization for texture mapping*, IEEE Transaction of Visualization and Computer Graphics, 6, 181-189, 2000.
[4] O. Lyttelton, M. Boucher, S. Robbins, and A. Evans, *An unbiased iterative group registration template for cortical surface analysis*, NeuroImage, Vol 34, 15351544, 2007.
[5] F. Gardiner and N. Lakic. *Quasiconformal Teichmuller Theory.* American Mathematics Society, 2000.
[6] B. Fischl, M. Sereno, R. Tootell, and A. Dale. High-resolution intersubject averaging and a coordinate system for the cortical surface. *Human Brain Mapping*, 8, 272-284, 1999.
[7] X. Gu, Y. Wang, T. F. Chan, P. M. Thompson, and S.-T. Yau. *Genus zero surface conformal mapping and its application to brain*, surface mapping. IEEE Transactions on Medical Imaging, 23(8), 949-958, 2004.
[8] Y. Wang, L. M. Lui, X. Gu, K. M. Hayashi, T. F. Chan, A. W. Toga, P. M. Thompson, and S.-T. Yau. Brain surface conformal parameterization using riemann surface structure. *IEEE Transactions on Medical Imaging*, 26(6), 853-865, 2007.
[9] X. Gu and S. Yau. *Computing conformal structures of surfaces*, Communication in Information System, 2(2), 121-146, 2002.
[10] S. Joshi and M. Miller. Landmark matching via large deformation diffeomorphisms. *IEEE Transactions on Image Processing*, 9(8), 1357-1370, 2000.
[11] J. Glaunès, M. Vaillant and M. I. Miller, *Landmark Matching via Large Deformation Diffeomorphisms on the Sphere*, Journal of Mathematical Imaging and Vision, 20, 179-200, 2004.
[12] J. Glaunes, L. Younes and A. Trouve, *Diffeomorphic matching of distributions: A new approach for unlabelled point-sets and sub-manifolds matching*, IEEE Computer Society Conference on Computer Vision and Pattern Recognition (CVPR'04), 2, 712–718, 2004.
[13] J. Glaunes, A. Qiu, M. Miller and L. Younes, *Large Deformation Diffeomorphic Metric Curve Mapping*, International Journal of Computer vision, 80(3), 317-336, 2008.
[14] J. Glaunes, A. Qiu, M. Miller and L. Younes, *Surface Matching via Currents*, Proceedings of Information Processing in Medical Imaging (IPMI'05), Vol. 3565, 381-392, 2005.
[15] M. K. Hurdal and K. Stephenson. *Discrete conformal methods for cortical brain flattening*, Neuroimage, 45, 86-98, 2009.
[16] N.A. Lord, J. Ho, B.C. Vemuri and S. Eisenschenk. *Simultaneous Registration and Parcellation of Bilateral Hippocampal Surface Pairs for Local Asymmetry Quantification*, IEEE Transactions on Medical Imaging, 26(4), 471478, 2007.
[17] T. Vercauteren, X. Pennec, A. Perchant and N. Ayache. *Diffeomorphic demons: Efficient non-parametric image registration.*, NeuroImage, 45(1), S61S72, 2009.
[18] B.T. Yeo, M.R. Sabuncu, T. Vercauteren, N. Ayache, B. Fischl, P. Golland. *Spherical demons: fast diffeomorphic landmark-free surface registration.*, IEEE Transactions on Medical Imaging, 29(3), 650668, 2010.
[19] F.L. Bookstein. *Principal Warps: Thin-Plate splines and the decomposition of deformations.*, IEEE Transactions on Pattern Analysis and Machine Intelligence, 11(6), 567-585, 1989.
[20] Y. Wang, L. Lui, T. Chan, and P. Thompson. Optimization of brain conformal mapping with landmarks. *Proceeding in Medical Image Computing and Computer-Assisted Internvention - MICCAI 2005*, 675-683, 2005.
[21] L. Lui, S. Thiruvenkadam, Y. Wang, T. Chan, and P. Thompson. *Optimized conformal parameterization of cortical surfaces using shape based matching of landmark curves*, Proceeding in Medical Image Computing and Computer-Assisted Internvention - MICCAI 2005, 494-502, 2008.
[22] L. Lui, S. Thiruvenkadam, Y. Wang, P. Thompson, and T. Chan. *Optimized conformal surface registration with shape-based landmark matching*, SIAM Journal of Imaging Sciences, 3(1), 52-78, 2010.
[23] L. Lui, Y. Wang, T. Chan, and P. Thompson. *Landmark constrained genus zero surface conformal mapping and its application to brain mapping research*, Applied Numerical Mathematics, 57, 847-858, 2007.
[24] L.M. Lui, Y. Wang, T.F. Chan, and P.M. Thompson. *Brain Anatomical Feature Detection by Solving Partial Differential Equations on General Manifolds*, Discrete and Continuous Dynamical Systems B, 7(3), 605-618, 2007
[25] L.M. Lui, T.W. Wong, X.F. Gu, T.F. Chan and S.T. Yau. *Compression of Surface Diffeomor-*

phism using Beltrami coefficient, IEEE Computer Vision and Pattern Recognition(CVPR), 2839-2846, 2010

[26] L.M. Lui, T.W. Wong, W. Zeng, X.F. Gu, P.M. Thompson, T.F. Chan and S.T. Yau. *Optimization of Surface Registrations Using Beltrami Holomorphic Flow*, Journal of Scientific Computing, 50(3), 557-585, 2012

[27] L.M. Lui, T.W. Wong, X.F. Gu, P.M. Thompson, T.F. Chan and S.T. Yau. *Hippocampal Shape Registration using Beltrami Holomorphic flow*, Medical Image Computing and Computer Assisted Intervention(MICCAI), Part II, LNCS 6362, 323-330 (2010)

[28] W. Zeng, L.M. Lui, F. Luo, T.F. Chan, S.T. Yau, X.F. Gu *Computing quasiconformal maps using an auxiliary metric and discrete curvature flow.* Numerische Mathematik, 121(4), 671-703, 2012

[29] L.M. Lui, K.C. Lam, T.W. Wong, X.F. Gu *Beltrami Representation and its applications to texture map and video compression.* arXiv:1210.8025 (http://arxiv.org/abs/1210.8025)

[30] O. Lehto and K. Virtanen. *Quasiconformal Mappings in the Plane.* Springer-Verlag, New York, 1973.

[31] R. Schoen and S.-T. Yau. *Lectures on Differential Geometry.* International Press of Boston, 1994.

[32] J. Foley, A. van Dam, S. Feiner and J. Hughes. *Computer Graphics*, Addison-Wesley Publishing, Massachusetts, 1992.

[33] P. S. Heckbert. *Survey of texture mapping*, IEEE Computer Graphics and Applications, 6(11), 5667, 1986.

[34] L. Balmelli, G. Taubin and F. Bernardini. *Space-optimised texture maps*, Computer Graphics Forum, 21(3), 411420, 2002.

[35] C. Bennis, J.M. Vézien and G. Iglésias. *Piecewise surface flattening for nondistorted texture mapping*, Computer Graphics (SIGGRAPH95 Proceedings) 25, 237246, 1991.

[36] S.D. Ma and H. Lin. *Optimal texture mapping*, EUROGRAPHICS88, pp 421428, September 1988.

[37] B. Levy and J.L. Mallet. *Non-Distorted Texture Mapping for Sheared Triangulated Meshes.* Computer Graphics (SIGGRAPH 98 Proceedings), 1998

[38] B. Levy. *Constrained Texture Mapping for Polygonal Meshes.* Computer Graphics (SIGGRAPH 98 Proceedings), 28, 2001

[39] D. Tosun, M. Rettmann and J. Prince. *Mapping techniques for aligning sulci across multiple brains.* Medical Image Analysis, 8, 295309, 2004

[40] W. Zeng and X. Gu. *Registration for 3D Surfaces with Large Deformations Using Quasi-Conformal Curvature Flow.* IEEE Conference on Computer Vision and Pattern Recognition (CVPR11), Jun 20-25, 2011, Colorado Springs, Colorado, USA.

[41] M. Jin, J. Kim, F. Luo and X. Gu. *Discrete surface Ricci flow.*. IEEE Transaction on Visualization and Computer Graphics, 14(5), 1030-1043, 2008

[42] Y.L. Yang, J. Kim, F. Luo, S. Hu, X.F. Gu *Optimal Surface Parameterization Using Inverse Curvature Map.* IEEE Transactions on Visualization and Computer Graphics , 14(5), 1054-1066, 2008.

[43] W. Zeng, L.M. Lui, L. Shi, D. Wang, W.C. Chu, J.C. Cheng, J. Hua, S.T. Yau, X.F. Gu. *Shape Analysis of Vestibular Systems in Adolescent Idiopathic Scoliosis Using Geodesic Spectra.* Medica Image Computing and Computer Assisted Intervation 13(3), 538-546, 2010.

[44] T. Lin, C.L. Guyader, I. Dinov, P. Thompson, A. Toga, L. Vese *Gene Expression Data to Mouse Atlas Registration Using a Nonlinear Elasticity Smoother and Landmark Points Constraints.* Journal of Scientific Computing, 50(3), 586-609, 2012.

[45] O. Weber, A. Myles, D. Zorin. *Computing Extremal Quasiconformal Maps.* Computer Graphics Forum, 31(5), 16791689, 2012

[46] Kurt Strebel. *On Quasiconformal Mappings of Open Riemann Surfaces. Comment. Math. Helvetici*, 53, 301-321, 1978.

[47] Edgar Reich. *Extremal Quasi-conformal Mappings of the Disk. Handbook of Complex Analysis: Geometric Function Theory*, Vol 1, Chapter 3, 75-135, 2002.